

---

# Cell-ontology guided transcriptome foundation model

---

Xinyu Yuan<sup>1,2</sup>, Zhihao Zhan<sup>1,2</sup>, Zuobai Zhang<sup>1,2</sup>, Manqi Zhou<sup>4</sup>

Jianan Zhao<sup>1,2</sup>, Boyu Han<sup>3</sup>, Yue Li<sup>1,3,\*</sup>, Jian Tang<sup>1,5,6,\*</sup>

<sup>1</sup>Mila - Québec AI Institute, <sup>2</sup>University of Montréal

<sup>3</sup>McGill University, <sup>4</sup>Cornell University, <sup>5</sup>HEC Montréal, <sup>6</sup>CIFAR AI Chair

\*Correspondence: yueli@cs.mcgill.ca; tangjian@mila.quebec

## Abstract

Transcriptome foundation models (TFMs) hold great promises of deciphering the transcriptomic language that dictate diverse cell functions by self-supervised learning on large-scale single-cell gene expression data, and ultimately unraveling the complex mechanisms of human diseases. However, current TFMs treat cells as independent samples and ignore the taxonomic relationships between cell types, which are available in cell ontology graphs. We argue that effectively leveraging this ontology information during the TFM pre-training can improve learning biologically meaningful gene co-expression patterns while preserving TFM as a general purpose foundation model for downstream zero-shot and fine-tuning tasks. To this end, we present **single cell, Cell-ontology guided TFM (scCello)**. We introduce cell-type coherence loss and ontology alignment loss, which are minimized along with the masked gene expression prediction loss during the pre-training. The novel loss component guide scCello to learn the cell-type-specific representation and the structural relation between cell types from the cell ontology graph, respectively. We pre-trained scCello on 22 million cells from CellxGene database leveraging their cell-type labels mapped to the cell ontology graph from Open Biological and Biomedical Ontology Foundry. Our TFM demonstrates competitive generalization and transferability performance over the existing TFMs on biologically important tasks including identifying novel cell types of unseen cells, prediction of cell-type-specific marker genes, and cancer drug responses.

## 1 Introduction

Cells are basic units of all living organisms. Deciphering diverse cell functions through gene expression is a long-standing challenge in life science and yet the essential path towards precision and personalized medicine. In this context, single-cell RNA sequencing (scRNA-seq) has emerged as a pivotal technique to measure the gene expression in individual cells. The vast amount of publicly available scRNA-seq data offers a rich transcriptomic data source [44] for learning cell representations towards various research applications, such as cancer therapy [56] and drug discovery [4].

Recently, several *Transcriptome Foundation Models* (TFMs) were developed to improve cell representation learning. They mainly utilize pre-training methods analogous to natural language processing like masked token prediction, treating genes as “tokens” and cells as “sentences” [14, 55, 63, 51]. However, the existing TFMs treat cells as independent samples and ignore their cell-type lineages. On the other hand, prior knowledge of the taxonomic relationships of cell types has been made available through the cell ontology graph by Open Biological and Biomedical Ontology Foundry [3]. Effectively leveraging the ontology knowledge can improve the quality of the pre-training on large-scale scRNA-seq atlases, which are heterogeneous and encompass hundreds of cell types. This can be done by training the TFM to recognize the inherent ontology relationships among cell types, thereby refining the cell representations. For instance, “mature  $\alpha$ - $\beta$  T cell” should be closer to “mature T

cells” compared to more general term “T cells” and farther from neurons and astrocytes from the brain (e.g., Tab. 7).

To capture this intuition, we propose scCello, a **single cell, Cell-ontology** guided TFM. scCello learns cell representation by integrating cell type information and cellular ontology relationships into its pre-training framework. scCello’s pre-training framework is structured with three levels of objectives: (1) **gene level**: a masked token prediction loss to learn gene co-expression patterns, enriching the understanding of gene interactions (Sec. 2.2); (2) **intra-cellular level**: an ontology-based cell-type coherence loss to encourage cell representations of the same cell type to aggregate, prompting consistency between cells and their types (Sec. 2.3); and (3) **inter-cellular level**: a relational alignment loss to guide the cell representation learning by consulting the cell-type lineage from the cell ontology graph (Sec. 2.4).

We demonstrate the generalizability and transferability of scCello on 22 million cells from CellxGene. For model generalization, we observe that scCello excels on cell type identification across all datasets in both zero-shot setting (i.e., directly using the pre-trained model) (Sec. 4.2.1) and fine-tuning setting (Sec. 4.2.2). In particular, scCello accurately classifies novel cell types by leveraging the ontology graph structure (Sec. 4.3). For transferability, scCello demonstrates competitive performances in predicting cell-type-specific marker genes (Sec. 4.4) and cancer drug responses (Sec. 4.5). Additionally, scCello is robust against batch effects (Sec. 4.6). Finally, we validate our contribution via ablation study (Sec. 4.7).

## 2 Method

Fig. 1 illustrates an overview of scCello. We present the details of individual components below.

### 2.1 Data Preprocessing

**Cell ontology graph.** Cell ontology is a widely used metadata schema for standard cell type annotations [16]. We downloaded the ontology from Open Biological and Biomedical Ontology Foundry (<https://obofoundry.org/>). It is structured as an unweighted directed acyclic graph  $\mathcal{G} = (\mathcal{V}, \mathcal{E})$ , where each node  $v \in \mathcal{V}$  corresponds to a distinct cell type and each directed edge  $(u, v) \in \mathcal{E}$  denotes a hierarchical lineage relationship of the form "is a subtype of" between cell types (Fig. 1a). To accurately represent the inherently symmetric "being biologically similar" relationship between cell types, the directed graph was transformed into an undirected one for subsequent calculation of cellular ontology relationships in Sec. 2.4.

**scRNA-seq data.** The scRNA-seq data were downloaded from CellxGene. After the preprocessing (App. B), we obtained 22 million cells. Each single-cell transcriptome is represented by a sequence of tuples, each containing genes and their expression counts.<sup>1</sup> Each sequence was then ordered by the rank of the gene expression values [55], akin to the sequential ordering of natural languages. Given a batch of  $B$  cells, each cell  $i \in \{1, \dots, B\}$  was assigned a cell type ontology identifier  $c_i \in \mathcal{V}$  from the CellxGene database, to enable mapping between cell and cell ontology.

### 2.2 Masked Gene Prediction

Same as BERT [15], scCello predicts a randomly masked gene token in each cell based on its surrounding context in the sequence. This objective  $\mathcal{L}_{\text{MGP}}$  aims to learn the dynamic gene co-expression network.

### 2.3 Intra-Cellular Ontology Coherence

A straightforward approach to encourage learning the cell representations that are coherent to the cell type labels is to apply cross-entropy loss for supervised cell type classification. However, this approach is limited in learning cell representation for the foundation model. Instead, we employed a supervised contrastive loss as our objective  $\mathcal{L}_{\text{Intra}}$ , which directly optimizes the TFM rather than

---

<sup>1</sup>scRNA-seq data was from CellxGene database <https://cellxgene.cziscience.com/>.

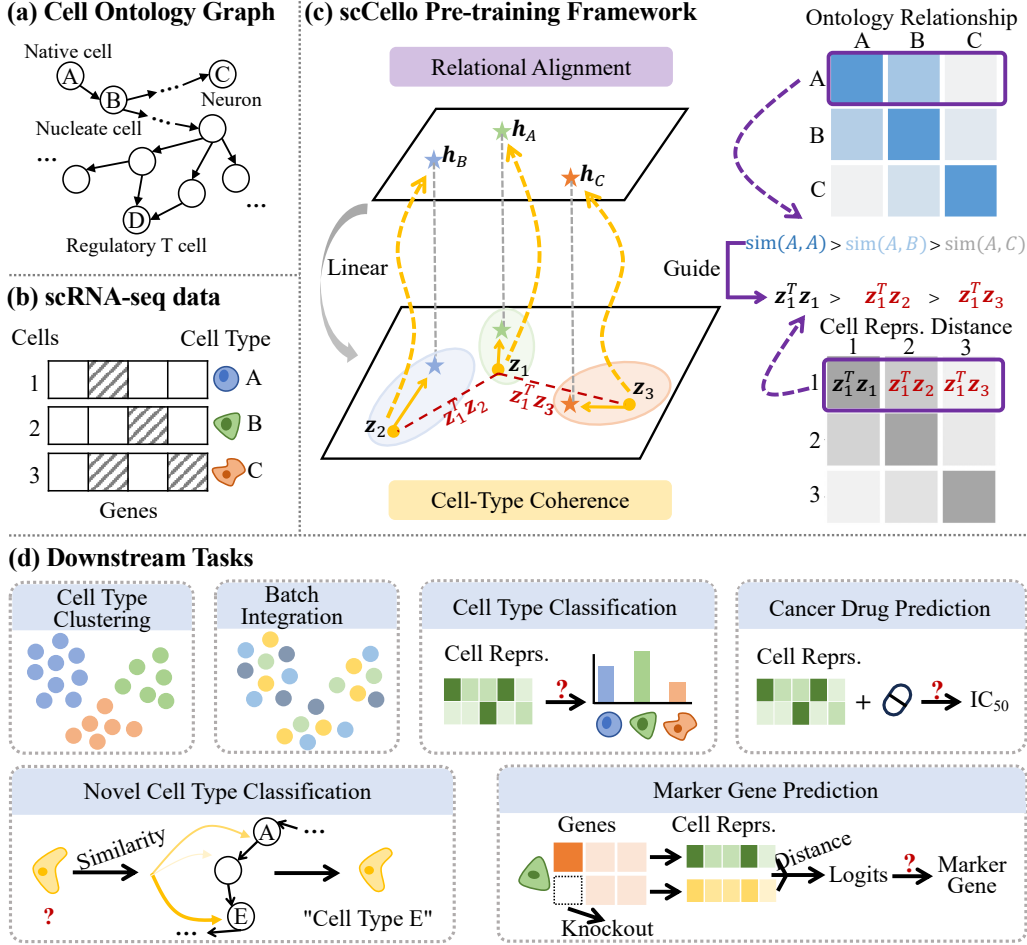


Figure 1: (a) Cell ontology graph describes taxonomic relationships between cell types. (b) Each cell in scRNA-seq data is represented by gene sequences, and associated with a cell type ontology identifier. (c) The pre-training framework of scCello is structured with three levels of objectives: gene-level masked gene prediction, intra-cellular level cell type coherence and inter-cellular level ontology alignment. For example, as shown in panel b, cells 1, 2, and 3 are labelled with cell type A, B and C. The intra-cellular cell type coherence loss encourages alignment of embedding  $z_1$  with  $h_A$ ,  $z_2$  with  $h_B$ , and  $z_3$  with  $h_C$ . The inter-cellular level ontology alignment loss encourages representational learning of cell similarities  $z_i^T z_j$  between cell  $i$  and  $j$  to be consistent to the similarity of their corresponding cell types  $sim(c_i, c_j)$  based on the ontology relationships. (d) Downstream tasks enabled by scCello and demonstrated in the study.

merely learning through the linear classifier:

$$\mathcal{L}_{\text{Intra}} = - \sum_{i=1}^B \log \left( \frac{\exp(z_i^T h_{c_i} / \tau)}{\exp(z_i^T h_{c_i} / \tau) + \sum_{j=1, j \neq i}^B \exp(z_i^T h_{c_j} / \tau)} \right). \quad (1)$$

where  $z_i$  and  $h_{c_i}$  denote the latent representation of cell  $i$  and cell type  $c_i$ , respectively.

This supervised contrastive loss pulls representations of the same class (positives) and repels representations of different classes (negatives). It often leads to representations that are at least as discriminative as the cross-entropy loss [22]. However, both cross entropy and contrastive loss are prone to class collapse, where all samples in a class are mapped to the same representation [30, 11]. The resulting model may produce simplistic representations that perform well on similar training tasks like cell type clustering or classification but generalize poorly to new tasks. This defeats the purpose of pre-training a versatile and general-purpose TFM. To tackle this limitation, we introduce a

regularization term  $\mathcal{L}_{\text{Reg}}$ :

$$\mathcal{L}_{\text{Reg}} = \sum_{i=1}^B \|\text{Linear}(\mathbf{h}_{c_i}) - \mathbf{z}_i\|_2^2, \quad (2)$$

where the linear layer is shared across all cells and cell types. Thereby, it constrains the cell type representation space to be an affine transformation of the cell representation space, thus reducing the degrees of freedom available for TFM optimization and the chance for class collapse.

## 2.4 Inter-Cellular Relational Alignment

To encourage TFMs to learn inter-cellular ontology relationships, scCello forces cell representations to truthfully reflect the pairwise node structural similarity derived from the cell ontology graph, using a relational alignment objective. This objective constitutes the most important part of scCello.

**Ontology relationships.** To effectively quantify ontology relationships between cell types from the ontology graph, scCello estimates pairwise node structural similarities as proxies using Personalized PageRank (PPR) [20]. PPR is a graph learning algorithm. The PPR score  $\text{PPR}(u, v)$  estimates the probability for a random walk. It starts from a given target node  $u \in \mathcal{V}$  and terminates at another node  $v \in \mathcal{V}$ . Importantly, this is a context-sensitive structural similarity measure that accounts both direct connections and broader subgraph patterns [60]. It also provides robustness against variations in global network structures, such as variable node degrees and clustering coefficients [10]. To improve robustness (as justified in App. A), we transform  $\text{PPR}(\cdot)$  through a non-linear function to derive the structural similarities  $\text{sim}(\cdot)$  as ontology relationships tunable by a hyper-parameter threshold  $s$ :

$$\text{sim}(u, v) = \begin{cases} \lfloor \log_2(\frac{\text{PPR}(u, v)}{s} + 1) \rfloor, & \text{if } \text{PPR}(u, v) \geq s \\ 1, & \text{otherwise} \end{cases}. \quad (3)$$

**Relational alignment.** Cells with closely related cell types tend to be more similar than those with distinct cell types. This observation guides scCello to align the distances between cell representations *w.r.t.* a target cell, with their structural similarities  $\text{sim}(\cdot)$  (as shown in Fig. 1c). Specifically, given a batch of  $B$  cells, if we consider a target cell  $i$  and another cell in the batch  $j \neq i$ , the representation distance  $\mathbf{z}_i^T \mathbf{z}_j$  should reflect their structural similarity  $\text{sim}(c_i, c_j)$ . Accordingly, a negative sample set  $\Omega_{i, j} = \{k | \text{sim}(c_i, c_j) > \text{sim}(c_i, c_k), 1 \leq k \leq B\}$  can be produced, where cell pair  $(i, k)$  are considered less similar to the cell pair  $(i, j)$  and should be contrasted against in the representation space using the objective  $\mathcal{L}_{\text{Inter}}$ :

$$\mathcal{L}_{\text{Inter}} = - \sum_{i=1}^B \sum_{j=1, j \neq i}^B \log \left( \frac{\exp(\mathbf{z}_i^T \mathbf{z}_j / \tau)}{\exp(\mathbf{z}_i^T \mathbf{z}_j / \tau) + \sum_{k \in \Omega_{i, j}} \exp(\mathbf{z}_i^T \mathbf{z}_k / \tau)} \right). \quad (4)$$

Notably, ancestor cell types, which can reach the target cell type via the directed "is a subtype of" edge on the ontology graph, are structurally distant from the target cell type. Despite being distant, they fall into the same, broader cell type category. Contrasting cells associated with these distant ancestor cell types with the target cell is counter-intuitive. Therefore, scCello explicitly excludes such cells from the negative sample set, avoiding inappropriately pushing away biologically similar cells. This enhances scCello’s capability to discern subtle similarities and differences within the cell types.

## 2.5 Overall Pre-training Objective

During pre-training, we seek to minimize the loss functions of all pre-training tasks simultaneously:

$$\theta^* \leftarrow \arg \min_{\theta} \mathcal{L}_{\text{MGP}} + \mathcal{L}_{\text{Inter}} + \mathcal{L}_{\text{Intra}} + \mathcal{L}_{\text{Reg}} \quad (5)$$

where  $\theta$  denotes all learnable parameters in scCello, which adopts transformer stacks as model backbones. We state the detailed information of model architectures in App. C.

## 3 Related Work

The rapid growth of scRNA-seq datasets has opened new avenues for constructing TFMs, enabling transfer learning across various biological downstream tasks. Initial efforts, such as scBERT [65],

Exceiver [13] and Geneformer [55], borrows the concept of masked language modeling [15] from natural language processing (NLP) domain for pre-training, by treating cells as sentences and genes as tokens. Concurrently, tGPT [54] and scGPT [14] explored generative modeling [49], and CellLM [67] adapted the idea of contrastive learning [38]. Following the concept of “scaling” towards emergent ability [63] in NLP, scFoundation [24] proposes the largest foundation model at the time in terms of model size and pre-training data size; scHyena [45] scales modeling context window size to the full length of scRNA-seq data with Hyena operator [47] instead of conventionally used transformers. scTab [18] is the first to explore large-scale supervised learning mechanism for scRNA-seq pre-training, and is capable of annotating unseen tissue cells for real-world applications. Moreover, SCimilarity [27] and UCE [51] focus on developing a unified latent space as a large-scale reference atlas for querying new cells. Yet, these TFMs mainly treat cells as independent samples during training and ignore their biological ontology relationships. scCello bridges this gap by incorporating cell type relationships derived from the cell ontology graph into TFM pre-training. This strengthens TFMs’ model generalization and transferability capability, as shown in Sec. 4.

## 4 Experiments

As an overview, the following experiments show that, **(1)** scCello can generalize to unseen cells, and to more difficult settings, such as cells of unseen cell types, tissues, and donors (Sec. 4.2.1); **(2)** scCello can benefit from fine-tuning on target datasets (Sec. 4.2.2); **(3)** the structural similarity embedded in scCello helps to classify novel cell types in a zero-shot manner (Sec. 4.3); **(4)** scCello effectively transfers to different downstream tasks (Sec. 4.4 and Sec. 4.5); **(5)** scCello is robust to batch effects that arise from different experimental conditions (Sec. 4.6); **(6)** Each loss component in Eqn. 5 is beneficial to scCello (Sec. 4.7). For every table reported, we used **bold** to highlight the best performance and results within 0.005 difference from the best. We used underlining to denote the second-best performances. For all metrics,  $\uparrow$  indicates the higher the better.

### 4.1 Setups

**Pre-training and downstream datasets.** We collected a large pre-training dataset consisting of 22 million cells along with downstream datasets. In particular, we generated one in-distribution (ID) and six out-of-distribution (OOD) datasets (App. B). The ID dataset is denoted as  $D^{id}$ . For the OOD setting, we introduced three scenarios: unseen cell types ( $\{D_i^{ct}\}_{i=1}^2$ ), unseen cell tissues ( $\{D_i^{ts}\}_{i=1}^2$ ), and unseen donors ( $\{D_i^{dn}\}_{i=1}^2$ ). Each scenario has two datasets. Notably, the OOD donor setting presents more realistic challenges than ID and other OOD settings because of the potential batch effects in the test donors.

**Pre-training configurations.** An Adam optimizer [35] (learning rate: 0.001, weight decay: 0.001, warm-up steps: 3, 333) was used to train the scCello for 40, 000 steps on 4 NVIDIA A100 GPUs on Compute Canada. We used 192 for batch size. More details are introduced in App. C.

**Baselines.** Across all downstream tasks, scCello is benchmarked with leading open-source large-scale TFMs: Geneformer [55], scGPT [14], scTab [18], UCE [51], and three TFM ablations. We also implemented ablated versions of scCello that only differ in the pre-training objectives from scCello: scCello using only the masked gene prediction loss (denoted as MGP), scCello using only the cell type supervised classification (denoted as Sup), and scCello using only the two losses (denoted as MGP+Sup). The three ablated TFMs provide a reference to isolate the effect of implementation details and training configurations. For each task, we also selected state-of-the-art non-TFM methods for fair comparison.

**Downstream metrics.** We evaluated the 3 tasks by the following metrics. (1) Clustering metrics include normalized mutual information (NMI), adjusted rand index (ARI), average silhouette width (ASW), and the average of the 3 scores (AvgBio) to assess both between-cluster separation and within-cluster closeness [14]. The batch integration task (Sec. 4.6) is evaluated by  $ASW_b$ , graph connectivity (GraphConn) and their average (AvgBatch), along with an overall score (Overall =  $0.6 \times \text{AvgBio} + 0.4 \times \text{AvgBatch}$ ) to balance biological relevance and batch consistency following [14]. (2) Classification metrics include accuracy (Acc), Macro F1 and area under the ROC curve (AU-ROC) [46]. (3) Regression task metrics include Pearson correlation coefficient score (PCC) [46]. Details for each metric were provided in App. D.1.

Table 1: Zero-shot cell type clustering on the curated ID and OOD datasets.

Method	In-Distribution (ID)				Out-of-Distribution (OOD)						
	$D^{id}$				$D_1^{ct}$	$D_2^{ct}$	$D_1^{ts}$	$D_2^{ts}$	$D_1^{dn}$	$D_2^{dn}$	OOD Avg.↑
	NMI↑	ARI↑	ASW↑	AvgBio↑	AvgBio↑	AvgBio↑	AvgBio↑	AvgBio↑	AvgBio↑	AvgBio↑	
<b>Non-TFM Methods</b>											
Raw Data	0.566	0.237	0.453	0.419	0.703	0.629	0.540	0.631	0.458	0.460	0.570
Seurat	0.648	0.270	0.407	0.442	0.752	0.737	0.587	0.636	0.466	0.489	0.611
Harmony <sup>1</sup>	0.621	0.261	0.382	0.421	0.432	0.417	0.462	0.515	0.456	0.474	0.459
scVI	0.660	0.297	0.464	0.474	0.760	0.725	0.577	0.634	0.478	0.502	0.613
<b>Ontology-Agnostic TFMs</b>											
Geneformer	0.616	0.261	0.418	0.432	0.689	0.668	0.539	0.597	0.468	0.482	0.574
scGPT	0.615	0.258	0.442	0.438	0.707	0.720	0.544	0.627	0.456	0.477	0.589
scTab	<u>0.707</u>	<u>0.479</u>	0.544	<u>0.577</u>	<u>0.759</u>	0.726	0.515	0.657	OOM	OOM	/
UCE	0.670	0.304	0.494	0.489	<b>0.772</b>	0.741	0.598	0.670	0.485	0.506	0.629
MGP	0.662	0.306	0.451	0.473	0.714	0.740	0.576	0.628	0.488	0.518	0.611
Sup	0.703	0.393	<u>0.569</u>	0.555	<b>0.767</b>	<u>0.775</u>	<u>0.605</u>	<u>0.680</u>	0.552	<u>0.573</u>	<u>0.659</u>
MGP+Sup	0.661	0.337	0.550	0.516	0.758	0.764	<b>0.610</b>	0.672	<u>0.553</u>	0.570	0.655
<b>Ontology-Enhanced TFMs</b>											
scCello	<b>0.785</b>	<b>0.558</b>	<b>0.667</b>	<b>0.670</b>	<b>0.769</b>	<b>0.786</b>	<b>0.612</b>	<b>0.705</b>	<b>0.608</b>	<b>0.643</b>	<b>0.687</b>

<sup>1</sup> Harmony could be over-corrected *w.r.t.* batch labels for datasets with many batches [9].

## 4.2 Cell Type Identification

### 4.2.1 Zero-shot Cell Clustering Results

**Setup.** For the cell type clustering task, TFM baselines and four non-TFM methods were evaluated: (1) raw data expressions of highly variable genes (*abbr.*, Raw Data) [33]; (2) Seurat [26]; (3) Harmony [36] (4) scVI [40]. Cell representations were extracted from the baselines and clustered by Louvain algorithm [5]. We evaluated the clustering performance of each method on both ID dataset  $D^{id}$  and OOD datasets  $D_i^{cond}$  ( $cond \in \{ct, ts, dn\}$ ,  $i \in \{1, 2\}$ ).

**ID and OOD generalization.** We reported zero-shot cell type clustering performance in Tab. 1, and included all the metrics for all datasets in App. D.2.1 due to space constraint. For both the ID and OOD settings, scCello consistently outperforms all baselines, achieving a 16.1% improvement in AvgBio on the ID dataset and a 12.1% improvement in average AvgBio across the six OOD datasets. Interestingly, while scCello outperforms non-TFM methods by a large margin, Geneformers and scGPT barely surpass these methods. The latter is consistent with previous observations [66].

In the OOD experiments, scCello confers strong generalization capability across unseen cell types tissue, and donors. In cell type clustering, scCello is the second best only trailing UCE by 0.03 and the best method for dataset 1 and 2. The OOD tissue setting highlights scCello’s ability to transfer its learned knowledge to different unseen tissues. Specifically, scCello achieve 0.6 and 0.7 while most methods conferred below 0.6 and 0.7 for the two datasets, respectively. For the unseen OOD donor scenario, most methods perform poorly with AvgBio ranging between 0.45 and 0.55. scCello led the chart achieving AvgBio above 0.6 in both datasets. Overall, scCello showcases strong model generalization capabilities across a range of biological conditions, which is attributable to the integration of cell ontology priors during its TFM pre-training. Indeed, the ablated models namely MGP, Sup, and MGP+Sup conferred lower scores compared to the full model.

### 4.2.2 Fine-tuning Results

**Setup.** We benchmarked all TFM baselines except UCE for its lack of fine-tuning support. These TFMs were fine-tuned on a subset of our pre-training data with supervised classification loss (details in App. D.2.2). We assessed both classification and clustering performance on the ID dataset  $D^{id}$ .

**Improvement with fine-tuning.** In Tab. 2, The fine-tuned scCello outperforms other TFMs on both classification and clustering metrics, achieving up to 25.9% improvement in Macro F1 over the best baseline. Moreover, scCello without fine-tuning still surpasses the performance of the other fine-tuned methods, further highlighting its superior transferability.

## 4.3 Novel Cell Type Classification

Novel cell type classification aims to label cells of unseen cell types without further fine-tuning. This task is useful for annotating completely new scRNA-seq datasets but infeasible for most of the

Table 2: Cell type identification using fine-tuned TFMs. Both the classification and clustering performances on the ID dataset  $D^{id}$  are reported.

Method	Classification		Clustering
	Acc $\uparrow$	Macro F1 $\uparrow$	AvgBio $\uparrow$
Scratch	0.621	0.223	0.544
<b>Ontology-Agnostic TFMs</b>			
Geneformer	0.747	0.440	0.439
scGPT	0.712	0.344	0.477
scTab	0.778	0.373	0.606
MGP	0.722	0.287	0.607
Sup	0.812	0.363	<u>0.659</u>
MGP+Sup	<u>0.820</u>	<u>0.406</u>	<u>0.607</u>
<b>Ontology-Enhanced TFMs</b>			
scCello	<b>0.867</b>	<b>0.511</b>	<b>0.694</b>

Table 3: Marker gene prediction, a binary classification task to identify cell-type-specific marker genes.

Method	$D_1^{mk}$	$D_2^{mk}$	Avg. $\uparrow$
	AUROC $\uparrow$	AUROC $\uparrow$	
<b>Ontology-Agnostic TFMs</b>			
Geneformer	0.452	0.470	0.461
scGPT	0.385	0.387	0.386
scTab	0.672	0.727	0.700
UCE	0.500	0.500	0.500
MGP	0.579	0.629	0.604
Sup	0.699	<u>0.693</u>	0.696
MGP+Sup	<u>0.730</u>	<b>0.730</b>	<u>0.730</u>
<b>Ontology-Enhanced TFMs</b>			
scCello	<b>0.756</b>	<b>0.729</b>	<b>0.743</b>

Table 4: Cancer drug response prediction: a regression task to predict the  $IC_{50}$  values of drugs.

Method	Non-TFM Methods		Ontology-Agnostic TFMs							Ontology-Enhanced TFMs
	DeepCDR	scFoundation	Geneformer	scGPT	scTab	UCE	MGP	Sup	MGP+Sup	scCello
PCC $\uparrow$	0.854	0.882	0.911	<b>0.919</b>	0.913	<b>0.922</b>	0.872	0.915	<u>0.916</u>	<b>0.917</b>

supervised methods that solely rely on the labels observed in the training data [7, 29, 61]. Leveraging the cell ontology graph that comprises the lineage relations among all of the known cell types, scCello makes this task feasible.

**Setup.** Our goal is to classify new query cells into "novel cell types" not seen during pre-training. To do this, we generate representations for both query cells and novel cell types, using similarity measures for classification. This process involves utilizing similarities between TFM-derived representations for the former and biological relationships from the cell ontology graph for the later. Details were described in App. D.3.

We benchmarked all TFMs and evaluated them on OOD cell type datasets  $D_1^{ct}$  and  $D_2^{ct}$ . We increased the difficulty of this task by the number of novel cell types (#Cell Types) that exist among the query cells. Specifically, we simulated five difficulty levels, with the number of novel cell types ranging from 10% to 100% of the total cell types. To assess the variance of the performance, we randomly sampled cell type combinations 20 times at each level.

**OOD generalization.** In Fig. 2, scCello led other TFMs by a large margin, achieving up to 76.8% Acc to classify 9 novel cell types (i.e., 10% of the total heldout cell types) and 33.5% Acc to classify up to 87 novel cell types (i.e., 100% of the total heldout cell types) (Tab. 16 and Tab. 17). These results show a significant leap from the existing TFMs, which either do not work or only work for annotating a handful of novel types [61, 41, 59].

#### 4.4 Marker Gene Prediction

Cell-type-specific genes, or marker genes, are highly expressed in a specific cell type but exhibit low expression in others. These genes play a crucial role in delineating cell functions in diverse tissue contexts. Identifying marker genes in less characterized cell types is an ongoing challenge [48].

**Setup.** We sought to assess whether the pre-trained TFMs can discriminate marker from non-marker genes for any cell type without any supervised fine-tuning. This zero-shot experiment evaluates whether the TFM is able to learn biologically meaningful gene co-expression patterns without supervision. For each cell, we quantified the marker gene potential of each gene by the changes in TFM-generated cell representations after *in-silico* knockout of the target gene (details in App. D.4). Here we assume that the larger the change the higher the marker gene potential. We discussed the caveat of this approach in Sec. 5. As test data, we used GSE96583 [31] ( $D_1^{mk}$ ) and GSE130148 [58] ( $D_2^{mk}$ ). We obtained the marker gene labels from CellMarker2 [28] and PanglaoDB [21].

**Zero-shot transferability.** In Tab. 3, scCello outperforms other TFMs, improving upon the second-best method by 1.8% in average AUROC. The inclusion of cell label information during pre-training boosts TFM performance, as evidenced by the strong results of scTab, Sup, MGP+Sup and scCello.

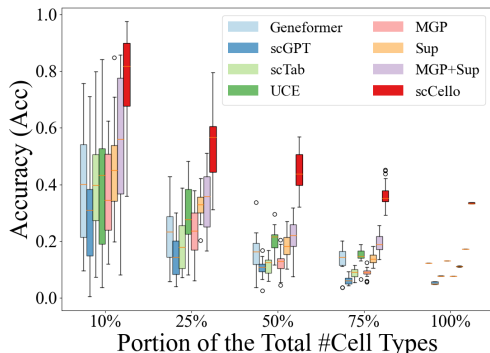


Figure 2: Novel cell type classification on OOD cell type dataset  $D_1^{ct}$  for increasing difficulties.

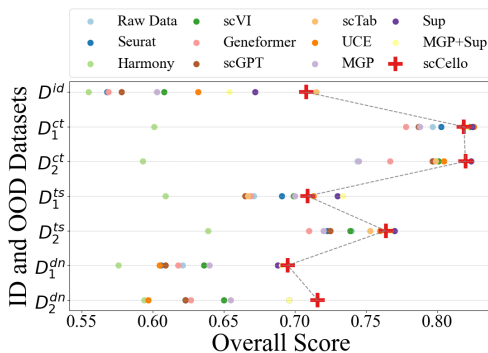


Figure 3: Batch integration on the curated ID and OOD datasets.

This is due to the biological correlation between marker genes and cell types. Furthermore, employing cell ontology graphs further improves the prediction accuracy over MGP+Sup.

#### 4.5 Cancer Drug Response Prediction

Developing effective drugs for cancer treatment is challenging due to individual variability in drug responses. Accurately predicting cancer drug responses (CDR) can greatly aid anti-cancer drug development and improve our understanding of cancer biology [39].

**Setup.** Following the approach of scFoundation [25], cell representations were extracted from fixed TFMs and integrated into the DeepCDR [39] pipeline to estimate the half-maximal inhibitory concentration ( $IC_{50}$ ) values of drugs (details in App. D.5). We benchmarked our method against DeepCDR, scFoundation, and other TFM baselines, using the same pre-processed data as DeepCDR.

**Zero-shot transferability.** In Tab. 4, scCello is among the top 3 along with scGPT and UCE, achieving 7.4% improvement in PCC over the base method DeepCDR. This highlights scCello’s transferability in enhancing specialized task-oriented methods. In particular, it can be used as a powerful feature extractor for diverse downstream tasks.

#### 4.6 Batch Integration

The scRNA-seq atlases, assembled from datasets across various labs and conditions, are prone to unwanted technical variations known as batch effects [42]. These effects can significantly affect the generalization ability of TFMs especially because they require pre-training on a massive amount of heterogeneous scRNA-seq data pooled from many studies. Here we sought to evaluate scCello’s robustness to batch effects without fine-tuning.

**Setup.** We adopted the same baselines as in zero-shot cell type clustering (Sec. 4.2.1), and followed the evaluation protocol of scGPT [14]. We evaluated on one ID dataset  $D^{id}$  and six OOD datasets  $D_i^{cond}$  ( $cond \in \{ct, ts, dn\}, i \in \{1, 2\}$ ) (see complete results of all metrics in App. D.6).

**Robustness to data noise.** Fig. 3 shows that scCello excels in 3 out of 7 datasets, and achieves comparable performance on another 3 datasets. The performance is attributable to the use of cell type information as the ablated baseline MGP conferred much lower batch integration score compared to Sup and scCello.

#### 4.7 Ablation Study

**Ablation of pre-training losses.** Tab. 5 reports the cell type clustering (Sec. 4.2.1) and novel cell type classification (Sec. 4.3) performance of scCello by using full or partial pre-training losses. Removing any of the four losses in Eqn. 5 resulted in decreased performance, corroborating the benefits of the proposed pre-training losses. Notably, removing the inter-cellular ontology relation loss  $\mathcal{L}_{Inter}$  led to 56.1% and 65.3% decrease in terms of Acc. and Macro F1 on novel cell type classification task, respectively. This shows the upmost importance of the structurally induced loss and ultimately the use of cell ontology graph information.



Table 5: Pre-training loss ablation on the cell type clustering and novel cell type classification (*abbr.*, "clf.") tasks.

Config	Cell Type Clustering		Novel Cell Type Clf.	
	$D_2^{ct}$	$D_2^{dn}$	$D_1^{ct}$	
	AvgBio $\uparrow$	AvgBio $\uparrow$	Acc $\uparrow$	Macro F1 $\uparrow$
Full Loss	0.786	0.643	0.335	0.150
w/o $\mathcal{L}_{MGP}$	0.774 ( $\downarrow 1.5\%$ )	0.640 ( $\downarrow 0.5\%$ )	0.287 ( $\downarrow 14.3\%$ )	0.131 ( $\downarrow 12.7\%$ )
w/o $\mathcal{L}_{Inter}$	0.778 ( $\downarrow 1.0\%$ )	0.620 ( $\downarrow 3.6\%$ )	0.147 ( $\downarrow 56.1\%$ )	0.052 ( $\downarrow 65.3\%$ )
w/o $\mathcal{L}_{Intra}$	0.730 ( $\downarrow 7.1\%$ )	0.626 ( $\downarrow 2.6\%$ )	0.280 ( $\downarrow 16.4\%$ )	0.118 ( $\downarrow 21.3\%$ )
w/o $\mathcal{L}_{Reg}$	0.764 ( $\downarrow 2.8\%$ )	0.638 ( $\downarrow 0.8\%$ )	0.296 ( $\downarrow 11.6\%$ )	0.134 ( $\downarrow 10.7\%$ )

Table 6: Overall performance v.s. the number of parameters.

Method	Perf. Rank	#Params (M)
Geneformer	6.3	<u>10.3</u>
scGPT	6.2	51.3
scTab	4.2	<b>9.7</b>
UCE	4.8	674.7
MGP	6.7	<u>10.3</u>
Sup	3.3	10.4
MGP+Sup	<u>3.2</u>	10.9
<b>scCello</b>	<b>1.3</b>	10.7

**Parameter efficiency.** Tab. 6 demonstrates that scCello is highly parameter-efficient, utilizing up to 60 times fewer parameters than the largest existing TFM, UCE, while still achieving the best average performance rankings across all downstream tasks. With an average performance rank of 1.3, scCello consistently ranks first or near the top in nearly every task.

**Visualization.** Visualization and analysis of scCello’s learned cell representations were presented in App. D.7. In short, biologically similar cell types are closer to each other and farther from those dissimilar ones in the t-SNE 2D space (Fig. 11).

## 5 Discussion and Conclusion

**Limitation and future work.** The cell ontology is constantly revised and expanded. In the future, we plan to investigate more efficient methods for fine-tuning scCello to enable continual learning of updated ontology, rather than retraining the entire model. Additionally, we aim to scale up the model size of scCello to increase its expressiveness and capacity. For the zero-shot marker gene prediction experiments (Sec. 4.4), one caveat is that our in-silico gene knockout approach also detects essential genes such as housekeeping genes [17] and transcription factors that are master regulators [8], which may not necessarily be marker genes. Nonetheless, deletion of these influential genes will also lead to large change of the transcriptome landscape of the cell. We will explore this in future study.

**Societal impact.** This work proposes a novel cell-ontology guided TFM, scCello, to enhance cell representation learning. On the positive side, once pre-trained, scCello can serve as a foundational model capable of facilitating scientific discoveries across various downstream tasks related to cells and cellular processes. However, on the negative side, the pre-training of scCello requires significant computational resources, potentially resulting in substantial carbon dioxide emissions that could contribute to environmental harm.

**Conclusion.** The proposed scCello incorporates cell ontology knowledge into its pre-training process by simultaneously modeling at the gene level, intra-cellular level, and inter-cellular level. We constructed a large-scale cell type identification benchmark to evaluate the model’s generalization capabilities, both in-distribution and out-of-distribution. Our evaluation demonstrates that scCello also exhibits strong transferability, as evidenced by its performance on other biologically meaningful downstream tasks such as zero-shot novel cell type classification and cell-type-specific marker gene prediction. Foundational models are typically heavy on the parameters for them to have sufficient capacity to learn from unlabeled data from scratch. This limits their usage to only fine-tuning tasks as pre-training them is prohibitive without large compute. Our proposed approach provides an efficient way of leveraging the prior knowledge at the pre-training, which led to much smaller parameter size while achieving performance comparable of the TFMs that are 5-60 times bigger. Together, scCello is a knowledge-informed and general purpose deep learning model that can be fine-tuned for a wide array of downstream applications, aiding in the rapid identification of novel cell types, disease-associated genes, and effective cancer drugs.

## Acknowledgments and Disclosure of Funding

The authors would like to thank Chence Shi, Meng Qu, Zhaocheng Zhu, and Sophie Xhonneux for their helpful discussions and comments. **We also appreciate all anonymous reviewers for their constructive suggestions, and plan to update the next version very soon.** This project is supported by Intel-MILA partnership program, the Natural Sciences and Engineering Research

Council (NSERC) Discovery Grant, the Canada CIFAR AI Chair Program, collaboration grants between Microsoft Research and Mila, Samsung Electronics Co., Ltd., Amazon Faculty Research Award, Tencent AI Lab Rhino-Bird Gift Fund and a NRC Collaborative R&D Project (AI4D-CORE-06). This project was also partially funded by IVADO Fundamental Research Project grant PRF-2019-3583139727. Y.L. is supported by Canada Research Chair (Tier 2) in Machine Learning for Genomics and Healthcare (CRC-2021-00547) and Natural Sciences and Engineering Research Council(NSERC) Discovery Grant (RGPIN-2016-05174). The computation resource of this project is supported by Mila, Calcul Québec and the Digital Research Alliance of Canada.

## References

- [1] Shibla Abdulla, Brian D. Aevermann, Pedro Assis, Seve Badajoz, Sidney M. Bell, Emanuele Bezzi, Batuhan Cakir, Jim Chaffer, Signe Chambers, J. Michael Cherry, Tiffany Chi, Jennifer Chien, Leah Dorman, Pablo Garcia-Nieto, Nayib Gloria, Mim Hastie, Daniel Hegeman, Jason Hilton, Timmy Huang, Amanda Infeld, Ana-Maria Istrate, Ivana Jelic, Kuni Katsuya, Yang-Joon Kim, Karen Liang, Mike Lin, Maximilian Lombardo, Bailey Marshall, Bruce Martin, Fran McDade, Colin Megill, Nikhil Patel, Alexander V. Predeus, Brian Raymor, Behnam Robatmili, Dave Rogers, Erica Rutherford, Dana Sadgat, Andrew Shin, Corinn Small, Trent Smith, Prathap Sridharan, Alexander Tarashansky, Norbert Tavares, Harley Thomas, Andrew Tolopko, Meg Urisko, Joyce Yan, Garabet Yeretssian, Jennifer Zamanian, Arathi Mani, Jonah Cool, and Ambrose J. Carr. Cz cell×gene discover: A single-cell data platform for scalable exploration, analysis and modeling of aggregated data. *bioRxiv*, 2023.
- [2] Sercan Ö Arik and Tomas Pfister. Tabetnet: Attentive interpretable tabular learning. In *Proceedings of the AAAI conference on artificial intelligence*, volume 35, pages 6679–6687, 2021.
- [3] Jonathan Bard, Seung Y Rhee, and Michael Ashburner. An ontology for cell types. *Genome biology*, 6:1–5, 2005.
- [4] Nurken Berdigaliyev and Mohamad Aljofan. An overview of drug discovery and development. *Future medicinal chemistry*, 12(10):939–947, 2020.
- [5] Vincent D Blondel, Jean-Loup Guillaume, Renaud Lambiotte, and Etienne Lefebvre. Fast unfolding of communities in large networks. *Journal of statistical mechanics: theory and experiment*, 2008(10):P10008, 2008.
- [6] Felipe A. Vieira Braga, Gozde Kar, Marijn Berg, Orestes A. Carpaij, Krzysztof Polański, Lukas M. Simon, Sharon Brouwer, Tomás Gomes, Laura Hesse, Jian Jiang, Eirini Sofia Fasouli, Mirjana Efremova, Roser Vento-Tormo, Carlos Talavera-López, Marnix R. Jonker, Karen Affleck, Subarna Palit, Paulina M. Strzelecka, Helen V. Firth, Krishnaa T. Mahbubani, Ana Cvejic, Kerstin B. Meyer, Kouroush Saeb-Parsy, Marjan A. Luinge, Corry-Anke Brandsma, Wim Timens, Ilias Angelidis, Maximilian Strunz, Gerard H. Koppelman, Antoon J. M. van Oosterhout, Herbert B. Schiller, Fabian J Theis, Maarten van den Berge, Martijn C. Nawijn, and Sarah A. Teichmann. A cellular census of human lungs identifies novel cell states in health and in asthma. *Nature Medicine*, 25:1153 – 1163, 2019.
- [7] Maria Brbic, Marinka Zitnik, Sheng Wang, Angela Oliveira Pisco, Russ B. Altman, Spyros Darmanis, and Jure Leskovec. Mars: discovering novel cell types across heterogeneous single-cell experiments. *Nature Methods*, 17:1200 – 1206, 2020.
- [8] Sunny Sun-Kin Chan and Michael Kyba. What is a master regulator? *Journal of stem cell research & therapy*, 3, 2013.
- [9] Ruben Chazarra-Gil, Stijn van Dongen, Vladimir Yu Kiselev, and Martin Hemberg. Flexible comparison of batch correction methods for single-cell rna-seq using batchbench. *Nucleic acids research*, 49(7):e42–e42, 2021.
- [10] Fan Chen, Yini Zhang, and Karl Rohe. Targeted sampling from massive block model graphs with personalized pagerank. *Journal of the Royal Statistical Society Series B: Statistical Methodology*, 82(1):99–126, 2020.

- [11] Mayee Chen, Daniel Y Fu, Avanika Narayan, Michael Zhang, Zhao Song, Kayvon Fatahalian, and Christopher Ré. Perfectly balanced: Improving transfer and robustness of supervised contrastive learning. In *International Conference on Machine Learning*, pages 3090–3122. PMLR, 2022.
- [12] David Combe, Christine Largeron, Mathias Géry, and Előd Egyed-Zsigmond. I-louvain: An attributed graph clustering method. In *Advances in Intelligent Data Analysis XIV: 14th International Symposium, IDA 2015, Saint Etienne. France, October 22-24, 2015. Proceedings 14*, pages 181–192. Springer, 2015.
- [13] William Connell, Umair Khan, and Michael J Keiser. A single-cell gene expression language model. *arXiv preprint arXiv:2210.14330*, 2022.
- [14] Haotian Cui, Chloe X. Wang, Hassaan Maan, Kuan Pang, Fengning Luo, Nan Duan, and Bo Wang. scgpt: toward building a foundation model for single-cell multi-omics using generative ai. *Nature methods*, 2024.
- [15] Jacob Devlin, Ming-Wei Chang, Kenton Lee, and Kristina Toutanova. Bert: Pre-training of deep bidirectional transformers for language understanding. *arXiv preprint arXiv:1810.04805*, 2018.
- [16] Alexander D. Diehl, Terrence F. Meehan, Yvonne M. Bradford, Matthew H. Brush, Wasila M. Dahdul, David S. Dougall, Yongqun He, David Osumi-Sutherland, Alan Ruttenberg, Sirarat Sarntivijai, Ceri E. Van Slyke, Nicole A. Vasilevsky, Melissa A. Haendel, Judith A. Blake, and Christopher J. Mungall. The cell ontology 2016: enhanced content, modularization, and ontology interoperability. *Journal of biomedical semantics*, 7(44), 2016.
- [17] Eli Eisenberg and Erez Y Levanon. Human housekeeping genes, revisited. *TRENDS in Genetics*, 29(10):569–574, 2013.
- [18] Felix Fischer, David S Fischer, Evan Biederstedt, Alexandra-Chloé Villani, and Fabian J Theis. Scaling cross-tissue single-cell annotation models. *bioRxiv*, 2023.
- [19] Felix Fischer, David S. Fischer, Evan Biederstedt, Alexandra-Chloé Villani, and Fabian J. Theis. Scaling cross-tissue single-cell annotation models. *bioRxiv*, 2023.
- [20] Dániel Fogaras, Balázs Rácz, Károly Csalogány, and Tamás Sarlós. Towards scaling fully personalized pagerank: Algorithms, lower bounds, and experiments. *Internet Mathematics*, 2(3):333–358, 2005.
- [21] Oscar Franzén, Li-Ming Gan, and Johan LM Björkegren. Panglaodb: a web server for exploration of mouse and human single-cell rna sequencing data. *Database*, 2019:baz046, 2019.
- [22] Florian Graf, Christoph Hofer, Marc Niethammer, and Roland Kwitt. Dissecting supervised contrastive learning. In *International Conference on Machine Learning*, pages 3821–3830. PMLR, 2021.
- [23] Aric Hagberg, Pieter Swart, and Daniel S Chult. Exploring network structure, dynamics, and function using networkx. Technical report, Los Alamos National Lab.(LANL), Los Alamos, NM (United States), 2008.
- [24] Minsheng Hao, Jing Gong, Xin Zeng, Chiming Liu, Yucheng Guo, Xingyi Cheng, Taifeng Wang, Jianzhu Ma, Le Song, and Xuegong Zhang. Large scale foundation model on single-cell transcriptomics. *bioRxiv*, pages 2023–05, 2023.
- [25] Minsheng Hao, Jing Gong, Xin Zeng, Chiming Liu, Yucheng Guo, Xingyi Cheng, Taifeng Wang, Jianzhu Ma, Le Song, and Xuegong Zhang. Large scale foundation model on single-cell transcriptomics. *bioRxiv*, 2023.
- [26] Yuhan Hao, Tim Stuart, Madeline H Kowalski, Saket Choudhary, Paul Hoffman, Austin Hartman, Avi Srivastava, Gesmira Molla, Shaista Madad, Carlos Fernandez-Granda, et al. Dictionary learning for integrative, multimodal and scalable single-cell analysis. *Nature biotechnology*, 42(2):293–304, 2024.

- [27] Graham Heimberg, Tony Kuo, Daryle DePianto, Tobias Heigl, Nathaniel Diamant, Omar Salem, Gabriele Scalia, Tommaso Biancalani, Shannon Turley, Jason Rock, et al. Scalable querying of human cell atlases via a foundational model reveals commonalities across fibrosis-associated macrophages. *bioRxiv*, pages 2023–07, 2023.
- [28] Congxue Hu, Tengyue Li, Yingqi Xu, Xinxin Zhang, Feng Li, Jing Bai, Jing Chen, Wenqi Jiang, Kaiyue Yang, Qi Ou, et al. Cellmarker 2.0: an updated database of manually curated cell markers in human/mouse and web tools based on scrna-seq data. *Nucleic Acids Research*, 51(D1):D870–D876, 2023.
- [29] Aleksandr Ianevski, Anil K. Giri, and Tero Aittokallio. Fully-automated and ultra-fast cell-type identification using specific marker combinations from single-cell transcriptomic data. *Nature Communications*, 13, 2022.
- [30] Jiachen Jiang, Jinxin Zhou, Peng Wang, Qing Qu, Dustin Mixon, Chong You, and Zhihui Zhu. Generalized neural collapse for a large number of classes. *ArXiv*, abs/2310.05351, 2023.
- [31] Hyun Min Kang, Meena Subramaniam, Sasha Targ, Michelle Nguyen, Lenka Maliskova, Elizabeth McCarthy, Eunice Wan, Simon Wong, Lauren Byrnes, Cristina M Lanata, et al. Multiplexed droplet single-cell rna-sequencing using natural genetic variation. *Nature biotechnology*, 36(1):89–94, 2018.
- [32] Hyun Min Kang, Meena Subramaniam, Sasha Targ, Michelle Ly Thai Nguyen, Lenka Maliskova, Elizabeth E. McCarthy, Eunice Wan, Simon Wong, Lauren E. Byrnes, Cristina M. Lanata, Rachel E. Gate, Sara Mostafavi, Alexander Marson, Noah A. Zaitlen, Lindsey A. Criswell, and Chun Jimmie Ye. Multiplexed droplet single-cell rna-sequencing using natural genetic variation. *Nature biotechnology*, 36:89 – 94, 2017.
- [33] Kasia Zofia Kedzierska, Lorin Crawford, Ava Pardis Amini, and Alex X Lu. Assessing the limits of zero-shot foundation models in single-cell biology. *bioRxiv*, pages 2023–10, 2023.
- [34] Hadas Keren-Shaul, Ephraim Kenigsberg, Diego Adhemar Jaitin, Eyal David, Franziska Paul, Amos Tanay, and Ido Amit. Mars-seq2. 0: an experimental and analytical pipeline for indexed sorting combined with single-cell rna sequencing. *Nature protocols*, 14(6):1841–1862, 2019.
- [35] Diederik P Kingma and Jimmy Ba. Adam: A method for stochastic optimization. *arXiv preprint arXiv:1412.6980*, 2014.
- [36] Ilya Korsunsky, Nghia Millard, Jean Fan, Kamil Slowikowski, Fan Zhang, Kevin Wei, Yuriy Baglaenko, Michael Brenner, Po-ru Loh, and Soumya Raychaudhuri. Fast, sensitive and accurate integration of single-cell data with harmony. *Nature methods*, 16(12):1289–1296, 2019.
- [37] Samuel A Lambert, Arttu Jolma, Laura F Campitelli, Pratyush K Das, Yimeng Yin, Mihai Albu, Xiaoting Chen, Jussi Taipale, Timothy R Hughes, and Matthew T Weirauch. The human transcription factors. *Cell*, 172(4):650–665, 2018.
- [38] Phuc H Le-Khac, Graham Healy, and Alan F Smeaton. Contrastive representation learning: A framework and review. *Ieee Access*, 8:193907–193934, 2020.
- [39] Qiao Liu, Zhiqiang Hu, Rui Jiang, and Mu Zhou. Deepcdr: a hybrid graph convolutional network for predicting cancer drug response. *bioRxiv*, 2020.
- [40] Romain Lopez, Jeffrey Regier, Michael B Cole, Michael I Jordan, and Nir Yosef. Deep generative modeling for single-cell transcriptomics. *Nature methods*, 15(12):1053–1058, 2018.
- [41] Mohammad Lotfollahi, Mohsen Naghipourfar, Malte D. Luecken, Matin Khajavi, Maren Büttner, Marco Wagenstetter, Žiga Avsec, Adam Gayoso, Nir Yosef, Marta Interlandi, Sergei Rybakov, Alexander V. Misharin, and Fabian J Theis. Mapping single-cell data to reference atlases by transfer learning. *Nature Biotechnology*, 40:121 – 130, 2021.
- [42] Malte D. Luecken, Maren Büttner, Kridsakorn Chaichoompu, Anna Danese, Marta Interlandi, MF Mueller, D Strobl, Luke Zappia, Martin Dugas, Maria Colomé-Tatché, and F Theis. Benchmarking atlas-level data integration in single-cell genomics. *Nature Methods*, 19:41 – 50, 2020.

- [43] Malte D Luecken, Maren Büttner, Kridsakorn Chaichoompu, Anna Danese, Marta Interlandi, Michaela F Müller, Daniel C Strobl, Luke Zappia, Martin Dugas, Maria Colomé-Tatché, et al. Benchmarking atlas-level data integration in single-cell genomics. *Nature methods*, 19(1):41–50, 2022.
- [44] Colin Megill, Bruce Martin, Charlotte Weaver, Sidney Bell, Lia Prins, Seve Badajoz, Brian McCandless, Angela Oliveira Pisco, Marcus Kinsella, Fiona Griffin, et al. Cellxgene: a performant, scalable exploration platform for high dimensional sparse matrices. *bioRxiv*, pages 2021–04, 2021.
- [45] Gyutaek Oh, Baekgyu Choi, Inkyung Jung, and Jong Chul Ye. schyena: Foundation model for full-length single-cell rna-seq analysis in brain. *arXiv preprint arXiv:2310.02713*, 2023.
- [46] Fabian Pedregosa, Gaël Varoquaux, Alexandre Gramfort, Vincent Michel, Bertrand Thirion, Olivier Grisel, Mathieu Blondel, Peter Prettenhofer, Ron Weiss, Vincent Dubourg, et al. Scikit-learn: Machine learning in python. *the Journal of machine Learning research*, 12:2825–2830, 2011.
- [47] Michael Poli, Stefano Massaroli, Eric Nguyen, Daniel Y Fu, Tri Dao, Stephen Baccus, Yoshua Bengio, Stefano Ermon, and Christopher Ré. Hyena hierarchy: Towards larger convolutional language models. In *International Conference on Machine Learning*, pages 28043–28078. PMLR, 2023.
- [48] Yixuan Qiu, Jiebiao Wang, Jing Lei, and Kathryn Roeder. Identification of cell-type-specific marker genes from co-expression patterns in tissue samples. *Bioinformatics*, 37(19):3228–3234, 2021.
- [49] Alec Radford, Karthik Narasimhan, Tim Salimans, Ilya Sutskever, et al. Improving language understanding by generative pre-training. 2018.
- [50] William M Rand. Objective criteria for the evaluation of clustering methods. *Journal of the American Statistical association*, 66(336):846–850, 1971.
- [51] Yanay Rosen, Yusuf Roohani, Ayush Agrawal, Leon Samotorcan, Tabula Sapiens Consortium, Stephen R Quake, and Jure Leskovec. Universal cell embeddings: A foundation model for cell biology. *bioRxiv*, pages 2023–11, 2023.
- [52] Peter J Rousseeuw. Silhouettes: a graphical aid to the interpretation and validation of cluster analysis. *Journal of computational and applied mathematics*, 20:53–65, 1987.
- [53] Robert Salomon, Dominik Kaczorowski, Fatima Valdes-Mora, Robert E Nordon, Adrian Neild, Nona Farbehi, Nenad Bartonicek, and David Gallego-Ortega. Droplet-based single cell rnaseq tools: a practical guide. *Lab on a Chip*, 19(10):1706–1727, 2019.
- [54] Hongru Shen, Jilei Liu, Jiani Hu, Xilin Shen, Chao Zhang, Dan Wu, Mengyao Feng, Meng Yang, Yang Li, Yichen Yang, et al. Generative pretraining from large-scale transcriptomes for single-cell deciphering. *Science*, 26(5), 2023.
- [55] Christina V. Theodoris, Ling Xiao, Anant Chopra, Mark D. Chaffin, Zeina R Al Sayed, Matthew C. Hill, Helene Mantineo, Elizabeth M Brydon, Zexian Zeng, X. Shirley Liu, and Patrick T. Ellinor. Transfer learning enables predictions in network biology. *Nature*, 618:616–624, 2023.
- [56] Ander Urruticoechea, Ramon Alemany, J Balart, Alberto Villanueva, Francesc Vinals, and Gabriel Capella. Recent advances in cancer therapy: an overview. *Current pharmaceutical design*, 16(1):3–10, 2010.
- [57] Ashish Vaswani, Noam Shazeer, Niki Parmar, Jakob Uszkoreit, Llion Jones, Aidan N Gomez, Łukasz Kaiser, and Illia Polosukhin. Attention is all you need. *Advances in neural information processing systems*, 30, 2017.
- [58] Felipe A Vieira Braga, Gozde Kar, Marijn Berg, Orestes A Carpaij, Krzysztof Polanski, Lukas M Simon, Sharon Brouwer, Tomás Gomes, Laura Hesse, Jian Jiang, et al. A cellular census of human lungs identifies novel cell states in health and in asthma. *Nature medicine*, 25(7):1153–1163, 2019.

- [59] Hui Wan, Liang Chen, and Min Deng. scemail: Universal and source-free annotation method for scrna-seq data with novel cell-type perception. *Genomics, Proteomics & Bioinformatics*, 20:939 – 958, 2022.
- [60] Hanzhi Wang, Zhewei Wei, Junhao Gan, Sibao Wang, and Zengfeng Huang. Personalized pagerank to a target node, revisited. In *Proceedings of the 26th ACM SIGKDD International Conference on Knowledge Discovery & Data Mining*, pages 657–667, 2020.
- [61] Wenchuan Wang, Fan Yang, Yuejing Fang, Duyu Tang, Junzhou Huang, Hui Lu, and Jianhua Yao. scbert as a large-scale pretrained deep language model for cell type annotation of single-cell rna-seq data. *Nature Machine Intelligence*, 4:852 – 866, 2022.
- [62] Xiliang Wang, Yao He, Qiming Zhang, Xianwen Ren, and Zemin Zhang. Direct comparative analyses of 10x genomics chromium and smart-seq2. *Genomics, Proteomics and Bioinformatics*, 19(2):253–266, 2021.
- [63] Jason Wei, Yi Tay, Rishi Bommasani, Colin Raffel, Barret Zoph, Sebastian Borgeaud, Dani Yogatama, Maarten Bosma, Denny Zhou, Donald Metzler, et al. Emergent abilities of large language models. *arXiv preprint arXiv:2206.07682*, 2022.
- [64] F Alexander Wolf, Philipp Angerer, and Fabian J Theis. Scanpy: large-scale single-cell gene expression data analysis. *Genome biology*, 19:1–5, 2018.
- [65] Fan Yang, Wenchuan Wang, Fang Wang, Yuan Fang, Duyu Tang, Junzhou Huang, Hui Lu, and Jianhua Yao. scbert as a large-scale pretrained deep language model for cell type annotation of single-cell rna-seq data. *Nature Machine Intelligence*, 4(10):852–866, 2022.
- [66] Hongyu Zhao, Tianyu Liu, Kexing Li, Yuge Wang, and Hongyu Li. Evaluating the utilities of large language models in single-cell data analysis. 2023.
- [67] Suyuan Zhao, Jiahuan Zhang, and Zaiqing Nie. Large-scale cell representation learning via divide-and-conquer contrastive learning. *arXiv preprint arXiv:2306.04371*, 2023.

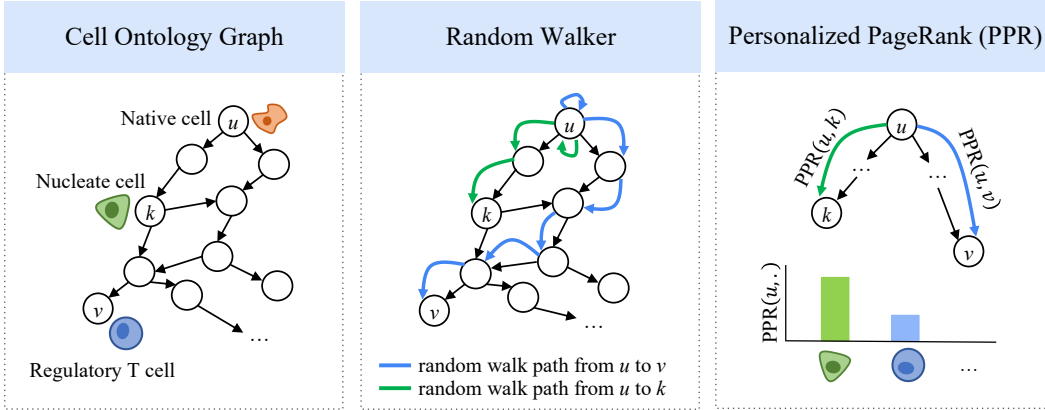


Figure 4: Graphical illustration of applying the Personalized PageRank (PPR) algorithm to cell ontology graph. As explained in App. A, PPR conducts random walks over the ontology graph with respect to a target cell type  $u$ , and converges to a steady state when the likelihood of terminating on each node stabilizes into a steady distribution. This likelihood distribution determines the final PPR score  $\text{PPR}(\cdot)$  and reflects the structural similarity between cell types.

## A PPR Transformation

**Personalized PageRank (PPR).** Personalized PageRank (PPR) extends the classic PageRank algorithm, which Google originally developed to rank web pages in search engines. PageRank conducts this by analyzing large-scale hyperlinked graphs on the web using random walker simulations. Unlike traditional PageRank that assigns a universal score to each web page, PPR customizes these scores. Specifically, individual user preferences during searches are incorporated, so that PPR can focus on web pages particularly relevant to each user. Due to its flexibility and effectiveness, PPR has been widely applied in graph learning across various fields, such as social networks, recommendation systems, and biological data analysis.

As illustrated in Fig. 4, this algorithm starts with a predefined preference node (or target node), which is emphasized according to the user’s interests. Subsequently, a random walk is conducted on the graph to facilitate graph traversal. At each step of the walk, there is a fixed probability  $\alpha$  that the walker will jump back to the target node from the current node instead of moving to an adjacent node chosen at random. This process of jumping, commonly referred to as "teleportation", biases the walk towards subgraphs that are of particular importance to the target node, thus personalizing the results according to user preferences. The walk continues until it reaches a steady state, at which point the likelihood of being on each node stabilizes into a steady-state distribution. These stabilized

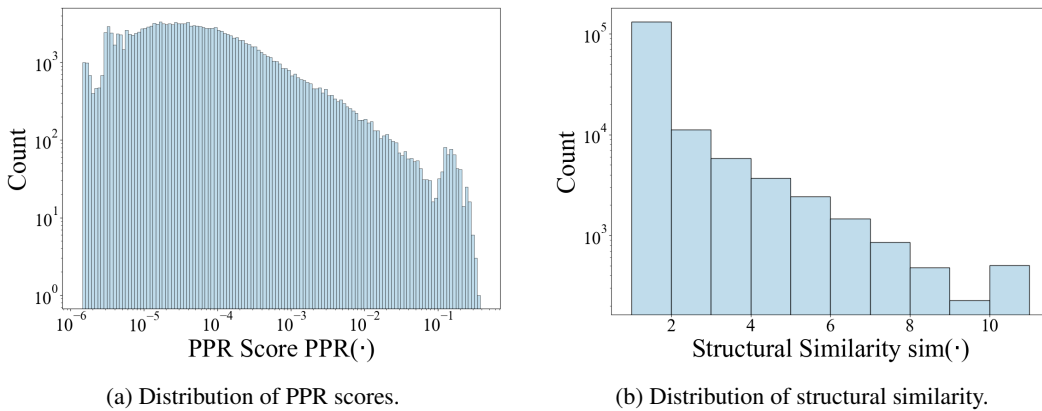


Figure 5: Comparison of the distributions for the PPR scores  $\text{PPR}(\cdot)$  and the structural similarity  $\text{sim}(\cdot)$  after the transformation.

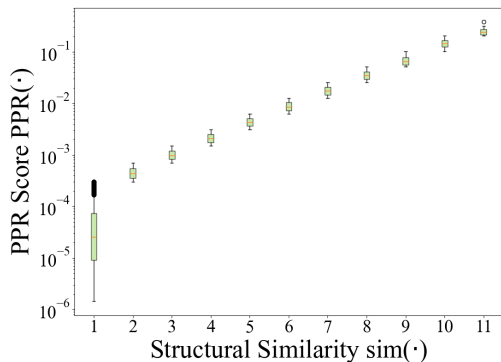


Figure 6: Relationships between the structural similarity  $\text{sim}(\cdot)$  after PPR transformation and the original PPR scores  $\text{PPR}(\cdot)$ .

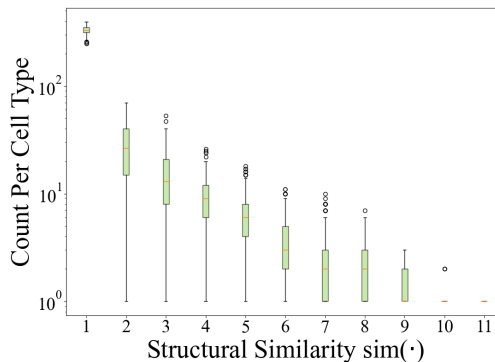


Figure 7: Frequency for each target cell type to be associated with other cell types that is at specific levels of structural similarity.

probabilities, reflecting both the graph’s structure and the user’s preferences, determine the PPR scores. These scores effectively evaluate each node’s structural similarities and rank them according to their relevance and importance from a personalized perspective.

**PPR transformation.** In scCello, the PPR algorithm is applied to the cell ontology graph to assess the structural similarities among cell types, or to measure their importance relative to a specified target cell type. We implemented PPR using the "pagerank" function in NetworkX [23] with "personalization" as arguments.

However, modification is needed to integrate PPR into TFM pre-training. The PPR scores are in real-number format and susceptible to numerical noise. Also, as shown in Fig. 5a, these scores typically exhibit a skewed distribution, concentrated around lower magnitudes. Consequently, setting precise thresholds to differentiate between node similarity and dissimilarity is challenging. Moreover, the vast amount small PPR values may be indistinguishable from noise.

To mitigate the effects of numerical noise and skewed magnitudes for the PPR scores, we employ truncation, logarithmic scaling, and discretization as outlined in Eqn. 3. Note that Eqn. 3 defines a monotonic, non-decreasing function that preserves the relative order between nodes. Its minimum value is set to 1 for the least similar cell types.

This equation transforms the raw PPR score,  $\text{PPR}(\cdot)$ , into the final structural similarity,  $\text{sim}(\cdot)$ . This transformation ensures that  $\text{sim}(\cdot)$  accurately reflects pronounced similarities as defined by the cell ontology and avoids emphasizing minor dissimilarities that could mislead during TFM pre-training.

**Analyses.** In Fig. 5, we present a comparison of the distributions for the PPR score,  $\text{PPR}(\cdot)$ , and the transformed structural similarity,  $\text{sim}(\cdot)$ . After transformation, the distribution of  $\text{sim}(\cdot)$  is less skewed and exhibits clear discretization. This facilitates the setting of definitive thresholds for distinguishing between similarity and dissimilarity among cell types, thereby enabling the effective incorporation of the cell ontology graph in scCello’s pre-training.

In addition, we provide detailed insights into the scale of structural similarity, the distribution of these similarities for each cell type, and examples of cell types associated with various levels of structural similarity:

- (1) Fig. 6 illustrates the correspondence between the structural similarity after PPR transformation and the original PPR scores, showcasing a log-linear relationship as expected. This helps clarify the scaling of structural similarity, which is discretized into integer levels ranging from 1 to 11.
- (2) Fig. 7 demonstrates how frequently each target cell type is associated with other cell types at specific levels of structural similarity. Consequently, during scCello’s pre-training, a substantial number of negative samples are expected to be utilized in the inter-cellular relational alignment objective, as outlined in Sec. 2.4.



Table 7: Examples of cell types associated with various levels of structural similarity,  $\text{sim}(\cdot)$ , for specified target cell types. Cell types demonstrated in the cell ontology graph in Fig. 1 are underlined.

Target Type	$\text{sim}(\cdot)$	Corresponding Cell Types
T Cell	8	"gamma-delta T cell", " <u>mature T cell</u> ", "lymphocyte"
	7	"mature gamma-delta T cell", " $\alpha$ - $\beta$ T cell", " <u>mature <math>\alpha</math>-<math>\beta</math> T cell</u> ", "thymocyte"
	6	"B cell", "double-positive, $\alpha$ - $\beta$ thymocyte", "CD8-positive, $\alpha$ - $\beta$ thymocyte", "CD4-positive, $\alpha$ - $\beta$ T cell", " <u>CD8-positive, <math>\alpha</math>-<math>\beta</math> T cell</u> ", "double negative thymocyte"
	5	"dendritic cell", "innate lymphoid cell", "plasmablast", "mononuclear cell", " <u>regulatory T cell</u> ", "memory T cell", "myeloid leukocyte", "naive T cell", "mature B cell", "CD4-positive, CD25-positive, $\alpha$ - $\beta$ regulatory T cell"
	...	...
	1	"renal intercalated cell", "smooth muscle fiber of ileum", "type II pneumocyte", "hematopoietic cell", " <u>neuron</u> ", "common lymphoid progenitor", ...
Neuron	7	"secretory cell"
	6	"glutamatergic neuron", "GABAergic neuron", "motor neuron", "neural cell", "peripheral nervous system neuron"
	5	"glycinergic neuron", "retinal bipolar neuron", " <u>native cell</u> ", "enteric neuron", "retina horizontal cell", "amacrine cell", "neuronal receptor cell"
	4	"retinal ganglion cell", "endocrine cell", "neuroendocrine cell", "cerebral cortex GABAergic interneuron", "muscle cell", "somatic cell"
	...	...
	1	"germ cell", " <u>T cell</u> ", "tracheal goblet cell", "DN3 thymocyte", "promonocyte", "cerebral cortex endothelial cell", ...

- (3) Tab. 7 displays examples of highly similar and dissimilar cell types categorized into various levels of structural similarity, specifically targeting "T cell" and "neuron" types.

## B Data Preprocessing Details

**Download and Preprocessing.** We downloaded from CellxGene [1] census version 2023-7-25. We focused on 291 datasets for human scRNA-seq. We preprocessed the dataset by the following steps:

- (1) **Remove non-primary cells.** Some data on CellxGene was duplicated due to multiple submissions of the same dataset from different research groups, therefore cells marked as "non-primary" were filtered out to prevent label leakage between pre-training and downstream.
- (2) **Filter out cells not produced by 10x-based [62] sequencing protocols.** There are numerous sequencing protocols in CellxGene database besides 10x-based sequencing [62], such as Drop-seq [53] and MARS-seq [34]. Only sequencing data from 10x-based sequencing protocols was kept to avoid large variation of data signals [42].
- (3) **Exclude cancer cells.** Cancer cells were highly dissimilar to normal cells and even occupied a large amount in the CellxGene database (nearly 12%). These cells could bring unexpected signals and skew the data, therefore we excluded these cancer cells.

To build downstream datasets for out-of-distribution (OOD) generalization evaluation, we first held out two category sets for each of the three settings: unseen cell types, unseen tissues and unseen

Table 8: Data statistics for our curated pre-training and downstream datasets, where the downstream datasets encompass one ID dataset and six OOD datasets under three different OOD scenarios, including unseen cell types, unseen tissues and unseen donors (Sec. 4.1). The blue colored numbers represent disjoint categories of that column. For example, in the "cell type" column, the cell type set in the pre-training data, and the cell type set in the OOD cell type dataset  $D_1^{ct}$  and  $D_2^{ct}$  are disjoint.

Dataset	#Total Cells	#Cell Types	#Tissues	#Donors	#Conditions	#Batches
Pre-training data	22,293,755	398	140	4,103	55	267
ID dataset $D^{id}$	22,317	318	132	3,447	54	261
OOD cell type dataset $D_1^{ct}$	486,810	87	125	122	35	90
OOD cell type dataset $D_2^{ct}$	435,791	87	128	106	40	117
OOD tissue dataset $D_1^{ts}$	335,675	186	32	1,801	10	28
OOD tissue dataset $D_2^{ts}$	341,681	205	32	2,052	7	25
OOD donor dataset $D_1^{dn}$	2,528,134	439	91	525	36	127
OOD donor dataset $D_2^{dn}$	2,521,868	404	101	525	33	123
In Total	/	572	204	5153	/	/

donors. Each category set were randomly selected with selection ratios 15%, 15% and 10% for the three OOD settings respectively. During the selection, we prohibited any category associated with more than 0.1% of the total pre-processed cells from being selected. This avoids losing too much data for pre-training. After the selection, cells associated with each held category set are collected, resulting in two OOD downstream datasets for each of the three OOD settings. These datasets are denoted as  $\{D_i^{ct}\}_{i=1}^2$  for the OOD cell type setting,  $\{D_i^{ts}\}_{i=1}^2$  for the OOD tissue setting, and  $\{D_i^{dn}\}_{i=1}^2$  for the OOD donor setting.

By excluding cells with at least one property belong to any of the six held category sets, the remaining data is further split into 99.9% as our pre-training data and 0.1% as the in-distribution (ID) downstream dataset  $D^{id}$ . This way, our pre-training data and the ID dataset  $D^{id}$  share similar data distributions.

**Data Statistics.** We summarize the data statistics for our curated pre-training dataset, one ID dataset and six OOD datasets in Tab. 8.

## C Implementation Details

**scRNA-seq Data.** scRNA-seq can enable the quantification of gene expression profiles of individual cells. Each cell’s gene expression profile can be described by the set  $\hat{X} = \{(e_1, g_1), (e_2, g_2), \dots, (e_M, g_M)\}$ , where  $e_k$  denotes the expression count of gene  $g_k$ , with  $e_k \geq 0$ . A value of  $e_k = 0$  indicates that the gene  $g_k$  is not expressed or not detected by the sequencing experiment. We use the same gene vocabulary set as [55], with the number of genes  $M=25,424$ .

**Gene Token Vocabulary.** The gene vocabulary set contains both protein-coding genes and miRNA genes.  $M$ , the number of genes, is not the same as the number of all tokens in the model vocabulary. scCello has  $M$  gene tokens plus three more special tokens [MASK] for masking, [CLS] for the start of a sentence and [PAD] for padding.

**Rank Value Encoding.** Unlike natural languages, which inherently follow a sequential order, scRNA-seq data presents a unique challenge due to the lack of intrinsic order among gene tokens. Therefore, we employ Rank Value Encoding [55] approach to rank genes based on their normalized expression set  $\{(\tilde{e}_i, g_i)\}_{i=1}^M$ . Specifically, gene expressions are first normalized by the total count within a cell [64] in a cell-wise manner, and then normalized through gene-specific weighting factors in a gene-wise manner. These factors are adopted from [55], which calculates the non-zero median value of expression of each detected gene across all cells. By design, these factors are assigned to emphasize lowly-expressed but essential genes, such as transcription factors [37], while deprioritizing ubiquitously expressed housekeeping genes [17].

After the normalization and ranking, it results in an ordered sequence of gene identities  $X = [g_{\pi(1)}, g_{\pi(2)}, \dots, g_{\pi(M)}]$  with an index permutation  $\pi(\cdot)$ , satisfying  $\tilde{e}_{\pi(1)} \geq \tilde{e}_{\pi(2)} \geq \dots \geq \tilde{e}_{\pi(M)}$ . To mitigate memory consumption, zero-expressed genes are removed and the gene sequence is

Table 9: Hyper-parameters comparison between TFM baselines (introduced in Sec. 4.1) and our TFM scCello. "The number of" is denoted with the symbol #.

Configuration	Geneformer [55]	scGPT [14]	scTab [19]	UCE [51]	scCello
#Parameters	10,316,196	51,330,049	9,655,628	674,745,857	10,683,654
Total GPUs	12 * V100 (32G)	4 * A100	1 * A100	24 * A100 (80G)	4 * A100 (40G)
Training Time	3 days	3 days	/	43.5 days	2 days
Sequence Length	2,048	1,200	19,331	1,024 [N]	2,048
Gene Mask Ratio	15%	/	/	20%	15%
Batch Size Per GPU	12	32	2,048	6	12
Gradient Accumulation Steps	1	1	1	4	4
Effective Batch Size	144	128	2048	576	192
Cell Reprs.	Avg. pooling	CLS	/	CLS	CLS
#Genes in Token Vocabulary	25,424	48,292	19,331	Any protein-coding genes	25,424
#Transformer Layers	6	12	/	33	6
Transformer Layer Hidden Dimension	512	512	/	5,120	512
Transformer Layer Embedding Size	256	512	/	1,280	256
#Transformer Heads	4	8	/	20	4
Transformer Layer Activation Function	GeLU	ReLU	/	ReLU	ReLU
MLP Layer Activation Function	ReLU	ReLU	/	GeLU	ReLU
Dropout	0.02	0.2	/	0.05	0.02

further truncated with a context length  $L=2,048$  in practice. This rank-based approach offers better robustness against technical artifacts than directly using the original numerical expressions, which can vary significantly in magnitude across different experimental assays [42].

**Cell and Cell Type Representations.** Given a pre-training dataset with  $N$  cells  $\mathcal{X} = \{X_1, X_2, \dots, X_N\}$ , each cell  $X_i$  can be mapped to a specific cell type ontology identifier  $c_i \in \mathcal{V}$ . For analyzing, scCello denotes cell  $X_i$ 's representation as  $z_i$  and cell type  $c_i$ 's representation as  $h_{c_i}$ .

**Masked Gene Prediction.** Given a batch of cells  $\{X_i\}_{i=1}^B$ , scCello predicts a gene token  $g_k$  based on the ordered gene sequence context  $X_{i,\setminus k}=[g_1, \dots, g_{k-1}, [\text{MASK}], g_{k+1} \dots, g_M]$  after replacing the token with a special [MASK]. This objective (term as  $\mathcal{L}_{\text{MGP}}$ ) aims to capture complex but important gene-gene interactions within one cell, like regulatory mechanisms between transcription factors and other genes:

$$\mathcal{L}_{\text{MGP}} = - \sum_{k=1}^B \mathbb{E}_{i \sim \Psi} - \log p(x_i | X_{k,\setminus i}) \quad (6)$$

where tokens are masked by a pre-defined distribution  $\Psi$ , same as that in BERT [15]. Specifically, 80% selected genes are replaced with [MASK], 10% selected genes are kept the same as its original, and 10% selected genes are replaced with random gene tokens.

**Model Architecture.** scCello utilizes a stack of self-attention transformer encoder layers [57], each composed of a self-attention and feedforward neural networks. The self-attention mechanism processes the input sequence, effectively capturing interactions between gene tokens.

**Configuration Hyper-parameters.** Besides scCello, we also summarize essential hyper-parameters for TFM baselines in Tab. 9 for comparison. It includes pre-training configurations like batch size,

Table 10: Metrics used in downstream tasks.

Task	Metrics
Cell Type Clustering (Sec. 4.2.1)	NMI, ARI, ASW, AvgBio
Cell Type Classification (Sec. 4.2.2)	Acc, Macro F1, AvgBio, $\Delta_{\text{AvgBio}}$
Novel Cell Type Classification (Sec. 4.3)	Acc, Macro F1
Marker Gene Prediction (Sec. 4.4)	AUROC
Cancer Drug Response Prediction (Sec. 4.5)	PCC
Batch Integration (Sec. 4.6)	NMI, ARI, ASW, AvgBio, ASW <sub>b</sub> , GraphConn, AvgBatch, Overall

sequence length, and training time consumed. It also includes architecture configurations for the transformer model backbone, such as the number of transformer layers and the embedding size of transformer layers. Note that scTab uses TabNet [2] instead of transformer layers as model backbone, therefore its architecture configurations are not recorded in the table.

## D Downstream Experiment Details

### D.1 Evaluation Metrics

All metrics used in downstream tasks are summarized in Tab. 10 and introduced below.

**Normalized Mutual Info Score (NMI).** The NMI is a metric that quantifies the similarity between two different clustering assignments or labelings of the same set of samples. We use NMI to compare the cell-type labels, with the cluster indices obtained from applying the Louvain clustering algorithm [12] on the target dataset.

We denote the two label assignments of the same  $N$  cell samples as  $C$  and  $K$ , representing the cell-type labels and the Louvain cluster indices, respectively. The entropy of a label assignment, say  $C$ , is a measure of the uncertainty associated with that assignment set. It’s calculated as:

$$H(C) = - \sum_{i=1}^{|C|} P(i) \log P(i) \quad (7)$$

where  $|C|$  is the number of unique cell types and  $P(i) = \frac{|C_i|}{N}$  is the probability that a randomly selected sample belongs to the class  $C_i$ . The entropy  $H(K)$  for the cluster indices  $K$  is computed similarly, with  $Q(j) = \frac{|K_j|}{N}$  being the probability of a sample belonging to the cluster  $K_j$ :

$$H(K) = - \sum_{j=1}^{|K|} Q(j) \log Q(j) \quad (8)$$

The mutual information (MI) between  $C$  and  $K$  quantifies the amount of information shared between the two label assignments. It is calculated by:

$$\text{MI}(C, K) = \sum_i^{|C|} \sum_j^{|K|} R(i, j) \log \frac{R(i, j)}{P(i)Q(j)} \quad (9)$$

where  $R(i, j) = \frac{|C_i \cap K_j|}{N}$  is the probability that a randomly selected sample belongs to both the class  $C_i$  and the cluster  $K_j$ .

The normalized mutual information (NMI) is defined as:

$$\text{NMI}(C, K) = \frac{\text{MI}(C, K)}{\text{mean}(H(C), H(K))} \quad (10)$$

NMI is a normalized version of MI, scaled by the mean of the entropy terms for cell-type labels and cluster indices. This normalization ensures that NMI values range from 0 to 1, where 0 indicates no correlation between the two label assignments, and 1 represents a perfect match.

To obtain the best match between the clusters and the cell-type labels, we performed optimized Louvain clustering over a range of resolutions from 0.1 to 2, in steps of 0.1. The clustering output with the highest NMI score, when compared to the cell-type label set, was selected as the optimal clustering result. The implementation of NMI used in this study was from the scib python library [43].

**Adjusted Rand Index Score (ARI).** The ARI is another metric used to evaluate the similarity between the clustering assignment and the cell type labels of the same set of samples, similar to the NMI metric. In this context, we similarly denote the cell-type labels as  $C$  and the Louvain [12] cluster indices computed on the target dataset as  $K$ .

The Rand Index (RI) is a measure of the overlap between the two clusterings,  $C$  and  $K$ . It considers both the correct clustering overlaps and the correct disagreements between the two clusterings [50]. Formally, if we define  $a$  as the number of pairs of elements that belong to the same set in both  $C$  and  $K$ , and  $b$  as the number of pairs of elements that are in different sets in  $C$  and in different sets in  $K$ , the unadjusted RI is given by:

$$\text{RI} = \frac{a + b}{C_2^N} \quad (11)$$

where  $N$  is the total number of cell samples and  $C_2^N$  represents the total number of possible pairs in the dataset.

However, the unadjusted RI does not account for the possibility of random label assignments leading to correct overlaps by chance. To address this issue, the adjusted RI (ARI) is introduced, which corrects for randomly correct labels by discounting the expected RI of random labelings:

$$\text{ARI} = \frac{\text{RI} - \mathbb{E}[\text{RI}]}{\max(\text{RI}) - \mathbb{E}[\text{RI}]} \quad (12)$$

The ARI ranges from 0 to 1, where 0 corresponds to a random labeling, and 1 indicates a perfect match between the two clustering assignments.

Similar to NMI, we performed NMI-optimized Louvain clustering to obtain the best match between the clusters and the cell-type labels. Specifically, we executed Louvain clustering over a range of resolutions and selected the clustering output with the highest NMI score when compared to the cell type label set. The implementation of ARI used in this study was from the scib python library [43].

**Average Silhouette Width Score (ASW).** The silhouette width [52] is a metric that evaluates the quality of a clustering solution by quantifying the relationship between the within-clustering distances and the between-cluster distances for each data point. Like the NMI and the ARI, the silhouette calculates the similarity between the clustering assignment and the cell type labels of the same set of samples.

For each cell sample, the silhouette width is computed based on two scores: (1)  $a$ : the mean distance between a sample and all other samples in the same cluster; and (2)  $b$  the mean distance between a sample and all samples in the nearest neighboring cluster. The silhouette score  $s_i$  for each sample  $i$  is defined as

$$s_i = \frac{b - a}{\max(a, b)} \quad (13)$$

The silhouette score ranges from -1 to 1, with higher values indicating that the sample is well-matched to its own cluster and dissimilar to the nearest neighboring cluster.

To obtain an overall assessment of the clustering quality, the average silhouette width (ASW) is calculated by averaging the silhouette scores  $s_i$  across all samples. This overall ASW, denoted as  $\text{ASW}_o$ , ranges between -1 and 1, with the following interpretations:

- $\text{ASW}_o$  close to 1: The clusters are dense and well-separated.

- $ASW_o$  around 0: The clusters overlap, and the between-cluster and within-cluster variability are approximately equal.
- $ASW_o$  near -1: Strong misclassification has occurred, where the within-cluster variability is greater than the between-cluster variability.

To ensure that the final ASW metric falls within the range of 0 to 1, a scaling operation is often applied:

$$ASW = \frac{ASW_o + 1}{2} \quad (14)$$

This scaled ASW value, ranging from 0 to 1, provides a convenient measure for evaluating the quality of the clustering solution, with higher values indicating better separation and cohesion of the clusters.

**AvgBio.** This score combines the three clustering metrics: NMI, ARI and ASW.

$$AvgBio = \frac{1}{3}(NMI + ARI + ASW) \quad (15)$$

**Silhouette Variant Score ( $ASW_b$ ).** To evaluate the effectiveness of the batch integration task (Sec. 4.6), a variant of the average silhouette width score (ASW) is employed, referred to as the  $ASW_b$ . Unlike  $ASW$  based on cell type labels,  $ASW_b$  considers batch labels. This score is designed to assess the degree of batch mixing, where a score of 0 indicates well-mixed batches, and deviations from 0 suggest the presence of a batch effect.

We take the absolute value of the original silhouette width score  $\tilde{s}_i$  for sample  $i$  based on batch labels:

$$s'_i = |\tilde{s}_i| \quad (16)$$

To ensure higher scores indicate better batch mixing, these scores are scaled by subtracting them from 1. As we expect batches to integrate within cell identity clusters, we compute the  $ASW_{b,j}$  score for each cell label  $j$  separately, using the following equation:

$$ASW_{b,j} = \frac{1}{|C_j|} \sum_{i \in C_j} 1 - s(i)' \quad (17)$$

where  $C_j = \{i | c_i = j\}_{i=1}^N$  is the set of cell indices whose cell type label is exactly  $j$ .

To obtain the final  $ASW_b$  score, the label-specific  $ASW_{b,j}$  scores are averaged across the set of unique cell type labels:

$$ASW_b = \frac{1}{|\mathcal{V}|} \sum_{j \in \mathcal{V}} ASW_{b,j} \quad (18)$$

where  $\mathcal{V}$  represents the set of unique cell type labels.

**Graph Connectivity (GraphConn).** The GraphConn metric is designed to assess whether the  $k$ -nearest neighbor ( $k$ NN) graph representation of the integrated data directly connects all cells with the same cell type label. This metric operates on the  $k$ NN graph, denoted as  $G_{kNN}$ , which is pre-processed by the Scanpy library using the "scanpy.pp.neighbors" function.

For each cell type label  $v \in \mathcal{V}$ , where  $\mathcal{V}$  represents the set of cell type labels (Sec. 2), a subset  $k$ NN graph  $G_{kNN}(\mathcal{V}_v; \mathcal{E}_v)$  is created. This subset graph contains only cells from the given label  $v$ .

Using these subset  $k$ NN graphs, the GraphConn score is computed as follows:

$$GraphConn = \frac{1}{|\mathcal{V}|} \sum_{v \in \mathcal{V}} \frac{|LCC(G_{kNN}(\mathcal{V}_v, \mathcal{E}_v))|}{|\mathcal{V}_v|} \quad (19)$$

Here,  $|LCC(\cdot)|$  is the number of nodes in the largest connected component of the graph and  $|\mathcal{V}_v|$  is the number of nodes with cell type  $v$ .

The resultant GraphConn score has a range of  $(0; 1]$ , where a score of 1 indicates that all cells with the same cell type are connected in the integrated  $k$ NN graph. The lowest possible score indicates a graph where no cell is connected to any other cell.

It's important to note that the GraphConn score is computed directly on the  $k$ NN graph representation of the integrated data. As a result, this metric can be used to evaluate the quality of any integration output, regardless of the specific integration method used.

**AvgBatch.** This score combines two metrics:  $ASW_b$  and GraphConn.

$$\text{AvgBatch} = \frac{1}{2}(ASW_b + \text{GraphConn}) \quad (20)$$

**Overall.** We follow scGPT [14] to calculate a weighted average score of both the batch removal score  $ASW_b$  and the bio-conservation score AvgBio to balance biological relevance and batch consistency, following the equation:

$$\text{Overall} = 0.6 * \text{AvgBio} + 0.4 * \text{AvgBatch} \quad (21)$$

**Accuracy (Acc).** In classification tasks like cell type classification (Sec. 4.2.2) and novel cell type classification (Sec. 4.3), we denote the predicted values of the  $i$ -th sample as  $\hat{y}_i$  and the corresponding true label as  $y_i$ . Then the accuracy metric is defined as

$$\text{Acc}(y, \hat{y}) = \frac{1}{N} \sum_{i=1}^N \mathbb{1}[\hat{y}_i == y_i] \quad (22)$$

where the  $\mathbb{1}[\cdot]$  is the indicator function.

**Macro F1 Score (Macro F1).** The F1 Score is essentially defined for binary classification tasks.

$$F_1 = \frac{2}{\text{Recall}^{-1} + \text{Precision}^{-1}} \quad (23)$$

$$\text{Recall} = \frac{\text{TP}}{\text{TP} + \text{FN}} \quad (24)$$

$$\text{Precision} = \frac{\text{TP}}{\text{TP} + \text{FP}} \quad (25)$$

where TP is the number of true positives, FN the number of false negatives, and FP the number of false positives. The recall is intuitively the ability of the classifier to find all the positive samples; The precision is intuitively the ability of the classifier not to label as positive a sample that is negative. For multi-class classification, macro F1 is defined as the average F1 taken over all different classes.

**ROC AUC Score (AUROC).** The Area Under the Receiver Operating Characteristic (AUROC) curve is a metric commonly used to evaluate the performance of binary classification models. It provides a comprehensive measure of the trade-off between the true positive rate (sensitivity) and the false positive rate (1 - specificity) across different classification thresholds.

In a binary classification task, the model’s output is typically a probability or score that represents the likelihood of a sample belonging to the positive class. By varying the classification threshold, different operating points on the ROC curve can be obtained, where each point represents a specific combination of true positive rate (TPR) and false positive rate (FPR).

The ROC curve is created by plotting the TPR (y-axis) against the FPR (x-axis) for different classification thresholds. The AUROC is then calculated as the area under this ROC curve, providing a single scalar value that summarizes the overall performance of the binary classifier. The AUROC ranges from 0 to 1, with the following interpretations: (1) AUROC=1 indicates perfect classification, where the classifier can perfectly distinguish between the positive and negative classes; (2) AUROC=0.5 indicates random guessing, indicating that the classifier performs no better than a random prediction.

The AUROC is a widely used metric because it provides a comprehensive evaluation of the classifier’s performance across all possible classification thresholds. It is invariant to class imbalance and does not require choosing a specific threshold, making it a robust and threshold-agnostic measure.

Furthermore, the AUROC has a statistical interpretation as the probability that a randomly chosen positive instance will have a higher predicted probability than a randomly chosen negative instance, which provides a clear interpretation of the metric’s value.

**Pearson correlation coefficient score (PCC).** The PCC is a widely used measure of the linear relationship between two variables. It quantifies the strength and direction of the linear association

between the variables, ranging from -1 to 1. The formula for the PCC between two variables, A and B, is given by:

$$r_{AB} = \frac{\sum_{i=1}^n (A_i - \bar{A})(B_i - \bar{B})}{\sqrt{\sum_{i=1}^n (A_i - \bar{A})^2} \sqrt{\sum_{i=1}^n (B_i - \bar{B})^2}}$$

where  $A_i$  and  $B_i$  are the individual observations of variables A and B, respectively.  $\bar{A}$  and  $\bar{B}$  are the sample means of A and B, respectively.  $n$  is the number of observations.

The numerator represents the covariance between A and B, which measures how much A and B vary together from their respective means. The denominator normalizes the covariance by the product of the standard deviations of A and B, ensuring that the correlation coefficient falls within the range of -1 to 1. The interpretation of this PPC metric is as follows: (1)  $r_{AB}=1$  indicates perfect positive linear correlation (as A increases, B increases proportionally); (2)  $r_{AB}=-1$  indicates perfect negative linear correlation (as A increases, B decreases proportionally); (3)  $r_{AB}=0$  indicates no linear correlation between A and B; (4)  $0 < |r_{AB}| < 1$  indicates that the strength of the linear correlation increases as the value approaches 1 (either positive or negative).

In the context of regression analysis, computing the PCC between each regressor (independent variable) and the target variable can provide insights into the linear relationships between the predictors and the response variable.

## D.2 Cell Type Identification

### D.2.1 Zero-shot Identification (*i.e.*, Cell Type Clustering)

**Method.** We here discuss the experimental details for Sec. 4.2.1. Cell representations extracted from each baseline model are used to compute the  $k$  nearest neighbor ( $k$ NN) graph using Scanpy’s standard protocols [64]. These representations and the  $k$ NN graph are then processed with Louvain clustering algorithms at various resolutions, ranging from 0.1 to 2 in steps of 0.1. The optimized clustering result is determined by the highest gained NMI score achieved across all the resolutions.

For implementation, we accelerated Louvain clustering by adopting RAPIDS, a software library that enhances data science pipelines by entirely utilizing NVIDIA GPUs instead of traditional CPUs. Additionally, we conducted ten iterations of dataset down-sampling and reported the averaged NMI, ARI, ASW, and AvgBio scores. This approach significantly reduced the time required to evaluate a dataset, such as  $D^{id}$ , from days to just a few minutes.

**Datasets.** As introduced in Sec. 4.2.1, we evaluate one ID dataset ( $D^{id}$ ) and six OOD datasets ( $D_i^{cond}$  with  $cond \in \{ct, ts, dn\}$  and  $i \in \{1, 2\}$ ) to demonstrate our model’s generalization capabilities. These evaluations address various scenarios involving unseen cells for comprehensive testing, including cells with distributions similar to our pre-training dataset, as well as those associated with unseen cell types, tissues, and donors.

**Hyper-parameters.** We used  $k = 15$  neighbors to compute the  $k$ NN graph, with node distances calculated using the euclidean distance between cell representations. The Louvain clustering used seed 0 as the random state and treated the  $k$ NN graph as unweighted and directed.

**Performance.** In Sec. 4.2.1, Tab. 1 reports only the AvgBio metric for six OOD datasets due to space constraints. Full metrics, including NMI, ARI, and ASW, are detailed in: (1) Tab. 11 for the two OOD cell type datasets ( $D_1^{ct}$  and  $D_2^{ct}$ ); (2) Tab. 12 for the two OOD tissue datasets ( $D_1^{ts}$  and  $D_2^{ts}$ ); and (3) Tab. 13 for the two OOD donor datasets ( $D_1^{dn}$  and  $D_2^{dn}$ ).

### D.2.2 Identification with Fine-tuning (*i.e.*, Cell Type Classification)

**Method.** In this setting, the TFMs are further fine-tuned by adding a simple linear layer atop their model backbones, which transforms the hidden representations into prediction logits. The dimensions of these logits correspond to the number of cell type classes predicted. Importantly, all model parameters, including those of the TFM backbone and the newly added linear layer, are trainable during fine-tuning. The model checkpoint that achieves the highest Macro F1 score on the validation data is then selected for final testing.



Table 11: Full results for the OOD unseen cell type datasets  $D_1^{ct}$  and  $D_2^{ct}$  in the cell type clustering.

Method	OOD CellType Data ( $D_1^{ct}$ )				OOD CellType Data ( $D_2^{ct}$ )			
	NMI↑	ARI↑	ASW↑	AvgBio↑	NMI↑	ARI↑	ASW↑	AvgBio↑
<b>Non-TFM Methods</b>								
Raw Data	0.864	0.718	0.529	0.703	0.823	0.557	0.505	0.629
Seurat	<u>0.893</u>	0.773	0.590	0.752	0.884	0.723	0.605	0.737
Harmony	0.553	0.241	0.432	0.432	0.594	0.248	0.411	0.417
scVI	<b>0.905</b>	<u>0.797</u>	0.577	<u>0.760</u>	0.889	0.709	0.577	0.725
<b>Ontology-Agnostic TFMs</b>								
Geneformer	0.846	0.697	0.525	0.689	0.846	0.629	0.530	0.668
scGPT	0.866	0.705	0.551	0.707	0.873	0.724	0.564	0.720
scTab	0.886	<b>0.807</b>	0.584	0.759	0.867	0.754	0.557	0.726
UCE	<b>0.902</b>	<b>0.802</b>	0.612	<b>0.772</b>	0.892	0.695	<b>0.635</b>	0.741
MGP	0.860	0.710	0.573	0.714	0.881	0.745	0.595	0.740
Sup	0.892	0.787	<u>0.621</u>	<b>0.767</b>	<b>0.910</b>	<u>0.793</u>	<u>0.622</u>	<u>0.775</u>
MGP+Sup	0.888	0.775	0.611	0.758	<u>0.901</u>	0.779	0.611	0.764
<b>Ontology-Enhanced TFMs</b>								
scCello	0.887	0.781	<b>0.640</b>	<b>0.769</b>	<b>0.909</b>	<b>0.817</b>	<b>0.632</b>	<b>0.786</b>

Table 12: Full results for the OOD unseen tissue datasets  $D_1^{ts}$  and  $D_2^{ts}$  in the cell type clustering.

Method	OOD Tissue Data ( $D_1^{ts}$ )				OOD Tissue Data ( $D_2^{ts}$ )			
	NMI↑	ARI↑	ASW↑	AvgBio↑	NMI↑	ARI↑	ASW↑	AvgBio↑
<b>Non-TFM Methods</b>								
Raw Data	0.733	0.405	0.481	0.540	0.800	0.585	0.508	0.631
Seurat	<u>0.777</u>	0.497	0.488	0.587	0.813	0.560	0.535	0.636
Harmony	0.649	0.302	0.436	0.462	0.684	0.400	0.460	0.515
scVI	0.774	0.443	0.516	0.577	0.816	0.550	0.537	0.634
<b>Ontology-Agnostic TFMs</b>								
Geneformer	0.736	0.412	0.468	0.539	0.787	0.499	0.505	0.597
scGPT	0.739	0.407	0.486	0.544	0.794	0.556	0.531	0.627
scTab	0.754	0.492	0.515	0.515	0.815	0.616	0.541	0.657
UCE	<b>0.787</b>	0.476	0.531	0.598	<b>0.836</b>	0.610	0.562	0.670
MGP	0.766	0.472	0.491	0.576	0.802	0.544	0.537	0.628
Sup	<b>0.788</b>	<u>0.502</u>	<u>0.527</u>	<u>0.605</u>	<b>0.838</b>	<u>0.621</u>	<u>0.580</u>	<u>0.680</u>
MGP+Sup	<b>0.789</b>	<b>0.518</b>	0.524	<b>0.610</b>	<u>0.833</u>	0.612	0.573	0.672
<b>Ontology-Enhanced TFMs</b>								
scCello	<b>0.784</b>	<b>0.519</b>	<b>0.534</b>	<b>0.612</b>	<b>0.839</b>	<b>0.675</b>	<b>0.601</b>	<b>0.705</b>

**Datasets.** We fine-tuned TFMs on a subset of our curated pre-training data, randomly selecting 90% for training and using the remaining 10% for validation. The final performance was tested on the ID dataset  $D^{id}$ , which consists of cell samples never seen during scCello’s pre-training. We explored two subset sizes, 0.1% and 1% of the pre-training data, to simulate scenarios where  $10\times$  more annotated data becomes available. This exploration is meaningful for real-world applications, where annotating data is both costly and time-consuming.

**Hyper-parameters.** For scCello, we set the following hyper-parameters for fine-tuning: a learning rate of  $5.0 \times 10^{-5}$ , a linear learning rate scheduler with 500 warmup steps, a weight decay of 0.001, and a batch size of 24. The same fine-tuning configuration was applied to the three ablation TFMs

Table 13: Full results for the OOD unseen donor datasets  $D_1^{dn}$  and  $D_2^{dn}$  in the Cell Type Clustering. Note that scTab is OOM on these two datasets.

Method	OOD Donor Data ( $D_1^{dn}$ )				OOD Donor Data ( $D_2^{dn}$ )			
	NMI↑	ARI↑	ASW↑	AvgBio↑	NMI↑	ARI↑	ASW↑	AvgBio↑
<b>Non-TFM Methods</b>								
Raw Data	0.665	0.247	0.462	0.458	0.665	0.251	0.462	0.460
Seurat	0.691	0.294	0.413	0.466	0.711	0.335	0.420	0.489
Harmony	0.679	0.286	0.405	0.456	0.690	0.324	0.408	0.474
scVI	0.699	0.269	0.466	0.478	0.722	0.311	0.471	0.502
<b>Ontology-Agnostic TFMs</b>								
Geneformer	0.666	0.303	0.434	0.468	0.686	0.327	0.433	0.482
scGPT	0.656	0.259	0.452	0.456	0.677	0.298	0.456	0.477
scTab	/	/	/	OOM	/	/	/	OOM
UCE	0.718	0.245	0.491	0.485	0.737	0.284	0.496	0.506
MGP	0.713	0.294	0.457	0.488	0.734	0.359	0.462	0.518
Sup	<u>0.754</u>	<u>0.357</u>	<u>0.545</u>	<u>0.552</u>	<u>0.768</u>	<u>0.395</u>	<u>0.556</u>	<u>0.573</u>
MGP+Sup	<u>0.754</u>	<u>0.373</u>	<u>0.532</u>	<u>0.553</u>	<u>0.768</u>	<u>0.398</u>	<u>0.544</u>	<u>0.570</u>
<b>Ontology-Enhanced TFMs</b>								
<b>scCello</b>	<b>0.774</b>	<b>0.426</b>	<b>0.625</b>	<b>0.608</b>	<b>0.794</b>	<b>0.486</b>	<b>0.649</b>	<b>0.643</b>

Table 14: Cell type identification with fine-tuning evaluated on the ID dataset  $D^{id}$ , as the pre-training subset data size for fine-tuning increases from 0.1% to 1% for the subset selection ratio.

Methods	Cell Type Classification		Cell Type Clustering
	Acc↑ (0.1% → 1%)	Macro F1↑ (0.1% → 1%)	AvgBio↑ (0.1% → 1%)
<b>Ontology-Agnostic TFMs</b>			
Geneformer	0.747 → 0.872	0.440 → 0.664	0.439 → 0.469
scGPT	0.712 → 0.862	0.344 → 0.636	0.477 → 0.481
scTab	0.778 → 0.773	0.373 → 0.455	0.606 → 0.589
MGP	0.722 → 0.861	0.287 → 0.639	0.607 → 0.631
Sup	0.812 → <u>0.902</u>	0.363 → 0.718	<u>0.659</u> → <u>0.668</u>
MGP+Sup	<u>0.820</u> → <u>0.902</u>	<u>0.406</u> → <u>0.735</u>	0.607 → 0.667
<b>Ontology-Enhanced TFMs</b>			
<b>scCello</b>	<b>0.867</b> → <b>0.910</b>	<b>0.511</b> → <b>0.761</b>	<b>0.694</b> → <b>0.699</b>

pre-trained using scCello’s codebase (MGP, Sup, and MGP+Sup). For other TFM baselines, we searched for the optimal learning rate to report the final performance.

**Performance.** In Sec. 4.2.2, we reported classification and clustering metrics for TFMs fine-tuned with the 0.1% subset of the pre-training data. Here, we extend our reporting to TFMs fine-tuned with 1% of a pre-training subset that is  $10 \times$  larger. We compare performances at these two subset selection ratios in Tab. 14. We observe that,

- (1) As the size of fine-tuning data increases, all TFMs except scTab show benefits and scCello achieves 48.9% improvement in Macro F1 when the data size gets  $10 \times$  larger. scTab’s underperformance may be related to its model capacity, as it employs a TabNet architecture [2]—unlike others that use the powerful standard Transformers [57].
- (2) Across both the classification and clustering metrics, scCello’s prevails other TFM baselines by a large margin. Remarkably, even when fine-tuned with a smaller 0.1% pre-training subset, scCello surpasses TFMs fine-tuned with a much larger 1% subset, achieving a 3.9%

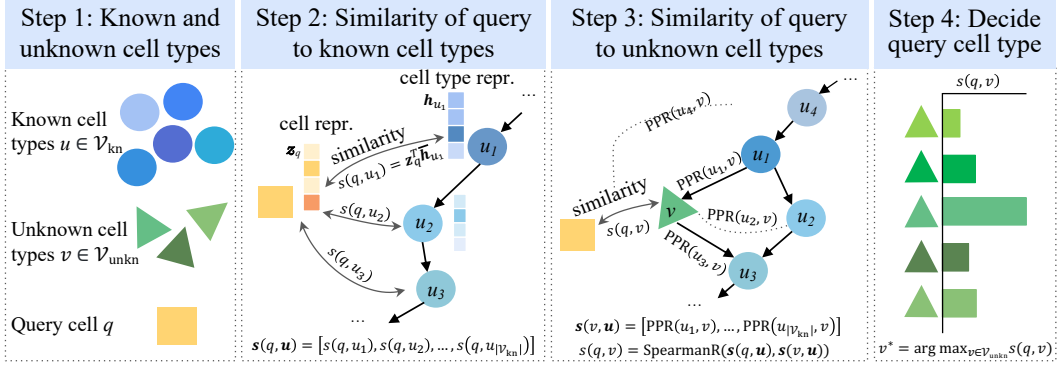


Figure 8: Graphical illustration of our approach for classifying novel cell types (*i.e.*, unknown cell types) (introduced in App. D.3).

improvement over the best baseline. This underscores scCello’s superiority, attributed to its cell-ontology guided pre-training.

- (3) Interestingly, clustering performance does not necessarily correlate directly with classification performance. For instance, while MGP+Sup outperforms Sup in classification metrics, it does not do so in clustering metrics. This observation underscores the importance to evaluate both the clustering and classification performances for cell type identification with model fine-tuning, which can make the evaluation setting more comprehensive and rigorous.

### D.3 Novel Cell Type Classification

**Method.** In this task, we define "known cell types"  $\mathcal{V}_{\text{kn}} \subseteq \mathcal{V}$  as the 398 cell types from our labeled pre-training dataset (see dataset statistics Tab. 8). "Novel cell types", or "unknown cell types"  $\mathcal{V}_{\text{unkn}} \subseteq \mathcal{V}$ , are those present only in the target downstream dataset and not observed during TFM pre-training ( $\mathcal{V}_{\text{unkn}} = \mathcal{V} \setminus \mathcal{V}_{\text{kn}}$ ).

Given a new query cell  $q$ , we aim to classify it to one of the unknown cell types  $\mathcal{V}_{\text{unkn}}$ . To solve this problem, we choose to first calculate representations for both the query cell sample and the unknown cell types. And then we measure the similarity between the two representations to determine the prediction results  $v_q \in \mathcal{V}_{\text{unkn}}$ .

Since unknown cell types are absent from the pre-training dataset, their representations cannot be directly obtained from any TFM baselines or our model, despite its ability to learn representations for known cell types. To address this problem, we leverage the known cell types  $\mathcal{V}_{\text{kn}}$  as a bridge to represent the query cells through the similarity between the cell and cell type representations produced by TFMs, and also represent the unknown cell types using the structural similarity relationships between the known and unknown ones derived from the cell ontology graph.

Specifically, our approach is illustrated in Fig. 8 and involves the following steps:

- (1) **Representations for known cell types.** Although scCello inherently learns cell type representations during pre-training, most existing TFMs do not output cell type representations directly. For benchmarking, we propose a protocol to calculate known cell type representations for general TFMs. Specifically, the representation for each known cell type is calculated by averaging cell representations derived from TFMs across cells belonging to this cell type. We used cell samples from a subset (10%) of our curated pre-training dataset, because the whole 22 million dataset is too large to fit.

We denote the known cell type representations as  $\{\bar{h}_u\}_{u \in \mathcal{V}_{\text{kn}}}$ , to differentiate with the notation of scCello’s learned cell type representations  $\{h_u\}_{u \in \mathcal{V}_{\text{kn}}}$  introduced in Sec. 2. For fair comparison, scCello also follows this protocol to generate known cell type representations, instead of using its learned ones. Nevertheless, we emphasize scCello’s capability to conduct this task alone without further accessing reference databases like our pre-training dataset.

- (2) **Similarity vector for a query cell to known cell types.** We first derive the cell representations for the query cell  $q$  from TFMs. Then, we estimate the similarity between the query cell  $q$  and any known cell type  $u \in \mathcal{V}_{\text{kn}}$  using the cosine similarity between their representations  $s(q, u) = \mathbf{z}_q^T \bar{\mathbf{h}}_u$ . For all known cell types, this results in a similarity vector:

$$\mathbf{s}(q, \mathbf{u}) = [d(q, u_1), d(q, u_2), \dots, d(q, u_{|\mathcal{V}_{\text{kn}}|})] \quad (26)$$

where we define the order of vector indices as  $\mathbf{u} = [u_1, u_2, \dots, u_{|\mathcal{V}_{\text{kn}}|}]$  satisfying  $u_1 < u_2 < \dots < u_{|\mathcal{V}_{\text{kn}}|}$ .

- (3) **Similarity vector for unknown cell types to known cell types.** For each unknown cell type  $v \in \mathcal{V}_{\text{unkn}}$ , we estimate the similarity  $s(v, \mathbf{u})$  between the unknown  $v$  and the known cell types  $\mathbf{u}$ . To achieve this, we leverage the cell ontology graph to calculate structural proximities as proxies. The proximities are measured using the raw PPR score  $\text{PPR}(u, v)$ ,  $u \in \mathcal{V}_{\text{kn}}, v \in \mathcal{V}_{\text{unkn}}$ , which is introduced in Sec. 2.4. Therefore, the similarity vector can be represented as:

$$\mathbf{s}(v, \mathbf{u}) = [\text{PPR}(u_1, v), \text{PPR}(u_2, v), \dots, \text{PPR}(u_{|\mathcal{V}_{\text{kn}}|}, v)], \quad (27)$$

- (4) **Align the similarity vectors for the query cell and the unknown cell types.** Intuitively, the similarity vector  $\mathbf{s}(q, \mathbf{u})$  indicates a profiling for the query cell  $q$ , with known cell types  $\mathbf{u}$  as a frame of reference; and the similarity vector  $\mathbf{s}(v, \mathbf{u})$  conveys similar profiling for an unknown cell type  $v$ . Therefore, the more similar the two similarity vectors  $\mathbf{s}(q, \mathbf{u})$  and  $\mathbf{s}(v, \mathbf{u})$  is, the higher possibility for the query cell to be alike this unknown cell type. We derive it using Spearman Ratio [46]  $\text{SpearmanR}(\cdot)$  as the similarity measure:

$$s(q, v) = \text{SpearmanR}(\mathbf{s}(q, \mathbf{u}), \mathbf{s}(v, \mathbf{u})). \quad (28)$$

Other formulas for the vector similarity function are available, like the commonly used cosine similarity (i.e.,  $d(q, v) = \mathbf{d}(q, \mathbf{u})^T \mathbf{s}(q, \mathbf{u})$ ). Our approach is not sensitive to the choice of the similarity metric. As shown in Fig. 10, using the dot product as the similarity score led to similar relative performance as in Fig. 2, where scCello generally performs better or on par with other TFMs. Therefore, we used Spearman Ratio throughout the experiments.

- (5) **Select the final answer.** The unknown cell type  $v^*$  with the largest distance is selected as the prediction for novel cell type classification:

$$v^* = \arg \max_{v \in \mathcal{V}_{\text{unkn}}} s(q, v) \quad (29)$$

In real-world applications, our approach is still applicable since almost all cell types are included in the cell ontology graph. But we won't be able to know whether the newly coming query cells are from unknown cell types  $\mathcal{V}_{\text{unkn}}$  or known cell types  $\mathcal{V}_{\text{kn}}$ . Therefore, we can expand the unknown cell type set  $\mathcal{V}_{\text{unkn}}$  to all the cell type defined in the ontology graph  $\mathcal{V}$ , and conduct similar processes in our approach.

**Datasets.** We evaluate on OOD cell type datasets  $D_1^{ct}$  and  $D_2^{ct}$ . The cell types in  $D_1^{ct}$  and  $D_2^{ct}$  are already aligned to the cell ontology graph using the ontology identifiers provided by CellxGene database, and are a subset of all the unknown cell types  $\mathcal{V}_{\text{unkn}}$ . We recognize that the prediction task becomes more challenging as the number of novel cell types increases. Therefore, we constrain the complete unknown cell type set to the cell types occurred in the datasets we used.

To further reflect the challenge, we created five difficulty levels, where the number of cell types spanned from 10%, 25%, 50%, 75% to 100% of the total cell type count. For example, if we use 25% cell types in the OOD cell type dataset  $D_1^{ct}$  with a total 87 cell types, the unknown cell types include ( $87 \times 25\% \approx 22$ ) randomly selected cell types from the complete set  $\{c_i | X_i \in D_1^{ct}\}$ . To account for potential biases, we randomly sampled 20 distinct combinations of cell types for each difficulty level.

**Hyper-parameters.** The  $\text{PPR}(\cdot)$  score is calculated using the "nx.pagerank" function with alpha hyper-parameter set to 0.9.

**Performance.** The full metrics for both accuracy and macro f1 score on the two OOD cell type datasets  $D_1^{ct}$  and  $D_2^{ct}$  are reported in Fig. 9. Besides plots, the numerical results are also summarized in Tab. 16 and Tab. 17 for reference.

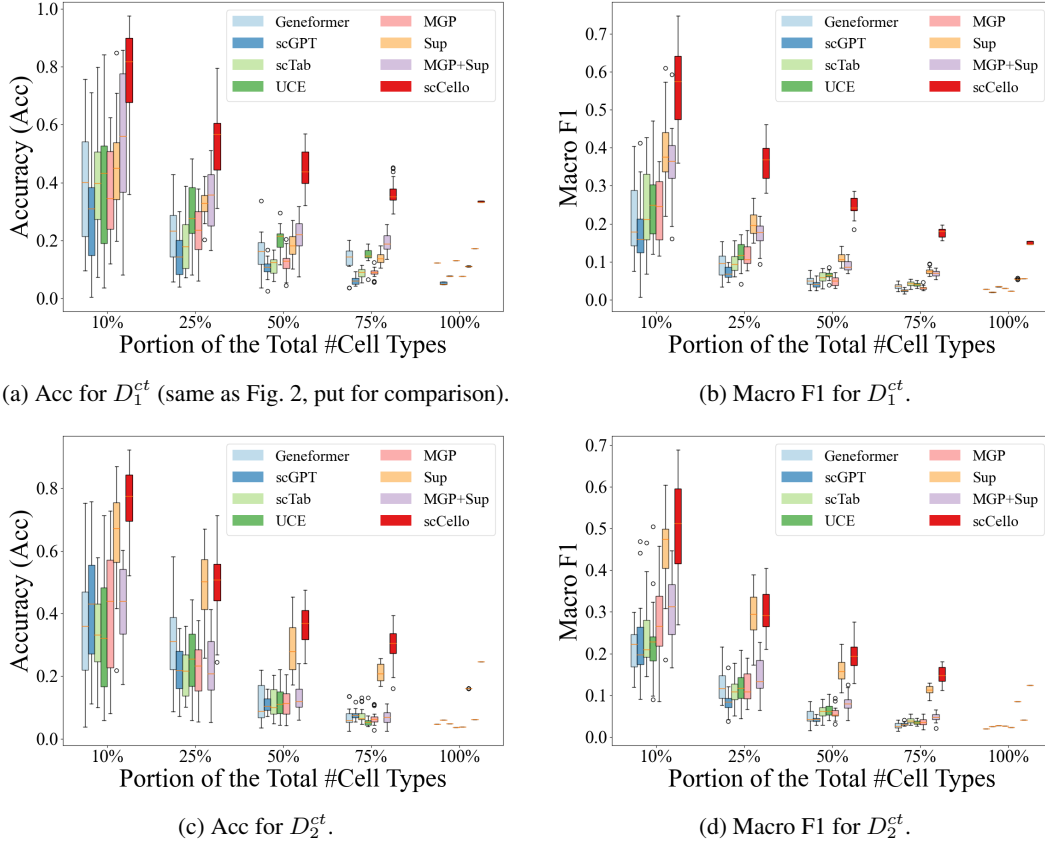


Figure 9: Novel cell type classification on two OOD cell type datasets  $D_1^{ct}$  and  $D_2^{ct}$ , using the Spearman Ratio similarity measure to compare the representations of the query cells and the novel cell types (App. D.3). Two metrics Acc and Macro F1 are reported.

Table 16: Novel cell type classification results on OOD cell type dataset  $D_1^{ct}$ .

Method	10% cell types		25% cell types		50% cell types		75% cell types		100% cell types	
	Acc $\uparrow$	F1 $\uparrow$	Acc $\uparrow$	F1 $\uparrow$	Acc $\uparrow$	F1 $\uparrow$	Acc $\uparrow$	F1 $\uparrow$	Acc $\uparrow$	F1 $\uparrow$
<b>Ontology-Agnostic TFMs</b>										
Geneformer	0.392	0.207	0.226	0.095	0.157	0.050	0.135	0.036	0.123	0.027
scGPT	0.291	0.178	0.148	0.072	0.105	0.041	0.062	0.024	0.052	0.020
scTab	0.380	0.248	0.191	0.096	0.114	0.058	0.088	0.042	0.077	0.035
UCE	0.399	0.253	0.289	0.120	0.205	0.064	0.149	0.040	0.131	0.030
MGP	0.361	0.243	0.233	0.119	0.125	0.048	0.089	0.032	0.076	0.022
Sup	0.464	<u>0.389</u>	0.329	<u>0.200</u>	0.187	<u>0.109</u>	0.139	<u>0.075</u>	0.111	0.055
MGP+Sup	<u>0.556</u>	0.358	<u>0.341</u>	0.172	<u>0.217</u>	0.089	<u>0.193</u>	0.069	<u>0.172</u>	<u>0.056</u>
<b>Ontology-Enhanced TFMs</b>										
scCello	<b>0.768</b>	<b>0.559</b>	<b>0.547</b>	<b>0.365</b>	<b>0.442</b>	<b>0.246</b>	<b>0.364</b>	<b>0.177</b>	<b>0.335</b>	<b>0.150</b>

#### D.4 Marker Gene Prediction

**Method.** We here explain our approach for this task in details. Given a cell’s gene expression profile, we enumerate each gene and attempt to knock it out, either by replacing it with a special [MASK] token or by reducing its expression to zero. The former method is used for Geneformer, MGP, Sup, MGP+Sup, and scCello, while the latter is applied to scGPT, scTab, and UCE. By comparing the cell representations of the mutated expression and those of the original expression, we assess the impact of each gene’s knockout. A greater impact suggests a higher likelihood of the gene being a

Table 17: Novel cell type classification results on OOD cell type dataset  $D_2^{ct}$ .

Method	10% cell types		25% cell types		50% cell types		75% cell types		100% cell types	
	Acc $\uparrow$	F1 $\uparrow$	Acc $\uparrow$	F1 $\uparrow$	Acc $\uparrow$	F1 $\uparrow$	Acc $\uparrow$	F1 $\uparrow$	Acc $\uparrow$	F1 $\uparrow$
<b>Ontology-Agnostic TFMs</b>										
Geneformer	0.367	0.213	0.310	0.125	0.107	0.048	0.069	0.027	0.047	0.020
scGPT	0.411	0.223	0.217	0.085	0.108	0.041	0.077	0.031	0.061	0.025
scTab	0.338	0.245	0.175	0.102	0.113	0.053	0.074	0.038	0.049	0.027
UCE	0.339	0.227	0.244	0.119	0.119	0.064	0.056	0.035	0.037	0.027
MGP	0.411	0.270	0.225	0.120	0.114	0.057	0.066	0.036	0.038	0.023
Sup	<u>0.581</u>	<u>0.372</u>	<u>0.325</u>	<u>0.204</u>	<u>0.199</u>	<u>0.112</u>	<u>0.140</u>	<u>0.081</u>	<u>0.108</u>	<u>0.063</u>
MGP+Sup	0.428	0.315	0.228	0.143	0.131	0.082	0.069	0.047	0.061	0.041
<b>Ontology-Enhanced TFMs</b>										
<b>scCello</b>	<b>0.763</b>	<b>0.500</b>	<b>0.498</b>	<b>0.304</b>	<b>0.364</b>	<b>0.196</b>	<b>0.297</b>	<b>0.149</b>	<b>0.247</b>	<b>0.124</b>

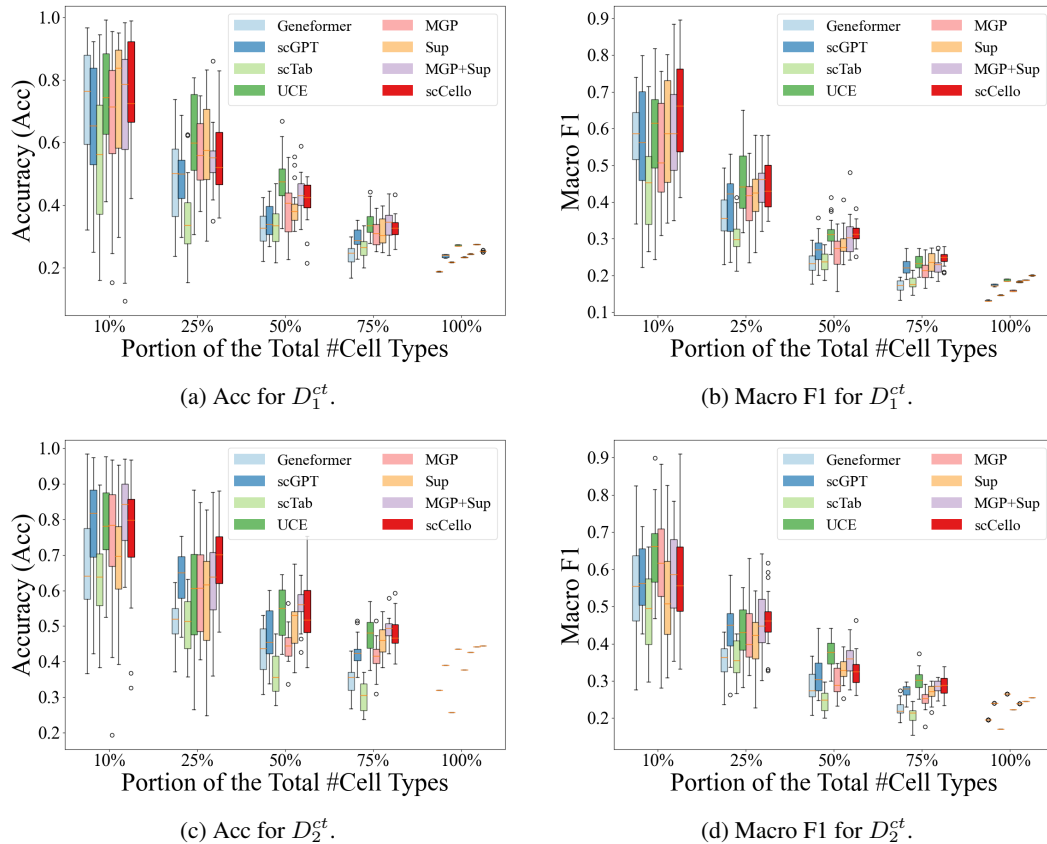


Figure 10: Novel cell type classification on two OOD cell type datasets  $D_1^{ct}$  and  $D_2^{ct}$ , using the cosine similarity measure to compare the representations of the query cells and the novel cell types (App. D.3). Two metrics Acc and Macro F1 are reported.

marker gene. This zero-shot approach requires no further fine-tuning and is particularly useful when additional computational resources or annotated datasets for fine-tuning are unavailable.

Notably, we acknowledge the shortage of our method: for house keeping genes (*i.e.*, non-marker genes), knocking out these genes will also have large impact on the cell because the cell would die [17]. Therefore, a high impact from gene knockout does not necessarily indicate a marker gene, but rather an "important" gene. However, this issue is not critical empirically, as the number of well-documented housekeeping genes is about 400, which is small compared to the extensive gene token vocabulary of  $M = 25,424$ .

Table 19: Full results for the five data subsets from GSE96583 ( $D_1^{mk}$ ) and one dataset from GSE130148 ( $D_2^{mk}$ ) in the marker gene prediction task (Sec. 4.4).

Method	GSE96583 ( $D_1^{mk}$ )					Avg.↑	GSE130148 ( $D_2^{mk}$ )	Avg.↑ of $D_1^{mk}$ and $D_2^{mk}$
	GSE96583_1 AUROC↑	GSE96583_2 AUROC↑	GSE96583_3 AUROC↑	GSE96583_4 AUROC↑	GSE96583_5 AUROC↑		AUROC↑	
<b>Ontology-Agnostic TFMs</b>								
Geneformer	0.445	0.447	0.478	0.484	0.408	0.452	0.470	0.461
scGPT	0.423	0.387	0.344	0.385	0.388	0.385	0.387	0.386
scTab	0.666	0.654	0.689	0.693	0.660	0.672	0.727	0.700
UCE	0.502	0.499	0.500	0.499	0.500	0.500	0.500	0.500
MGP	0.572	0.560	0.606	0.589	0.567	0.579	0.629	0.604
Sup	0.707	0.697	0.694	0.699	0.700	0.699	0.693	0.696
MGP+Sup	0.734	0.720	0.739	0.734	0.724	0.730	<b>0.730</b>	0.730
<b>Ontology-Enhanced TFMs</b>								
scCello	<b>0.767</b>	<b>0.753</b>	<b>0.754</b>	<b>0.748</b>	<b>0.760</b>	<b>0.756</b>	<b>0.729</b>	<b>0.743</b>

Table 20: Cell types for the two marker gene prediction datasets GSE96583 ( $D_1^{mk}$ ) and GSE130148 ( $D_2^{mk}$ ).

Dataset	Cell Types
GSE96583	"Dendritic cells", "CD8 T cells", "NK cells", "B cells", "Megakaryocytes", "FCGR3A+ Monocytes", "CD14+ Monocytes", "CD4 T cells", "Not Known"
GSE130148	"Macrophages", "T cell", "NK cell", "Mast cell", "Endothelium", "Lymphatic", "Pulmonary Alveolar Type II", "Transformed epithelium", "Ciliated", "Pulmonary Alveolar Type I", "B cell", "Fibroblast", "Secretory"

**Datasets.** As introduced in Sec. 4.4, we used the datasets from GSE96583 [32] and GSE130148 [6]. On the one hand, the GSE96583 dataset  $D_1^{mk}$  inherently contains five cell subsets associated with 9 cell type classes. The five cell subsets are denoted as "GSE96583\_1", "GSE96583\_2", "GSE96583\_3", "GSE96583\_4", "GSE96583\_5", respectively. On the other hand, the GSE130148 dataset  $D_2^{mk}$  contains 13 cell type classes. The size of these two datasets are summarized in Tab. 21, and their associated cell types are recorded in Tab. 20 for demonstration. Additionally, the ground truth cell-type-specific marker genes are originally sourced from two databases: CellMarker2 [28] and PanglaoDB [21].

**Performance.** In Sec. 4.4, we only reported the average performance across the 5 subsets of GSE96583 ( $D_1^{mk}$ ) and the individual performance of GSE130148 ( $D_2^{mk}$ ) in Tab 3. Here, we provide complete results for all five subsets in Tab. 19.

## D.5 Cancer Drug Response Prediction

**Method.** In this task, we first compute cell line level representations from scRNA-seq data and drug representations for associated drugs. Both these two representations are then input into the DeepCDR framework for training. Finally, we calculate the PCC between the predicted and actual IC50 values for each drug across all cell lines and report the average performance across all tested drugs.

Specifically, for TFMs, single-cell gene expression data are inputted into each model to generate cell-specific representations for each gene. These are then aggregated into cell line-level representations through max-pooling across all genes for each dimension. Conversely, the DeepCDR method uses raw gene expressions, aggregating them directly before max-pooling. Additionally, drugs are represented as graphs and encoded using graph neural networks to obtain drug representations.

**Datasets.** In our experiments, we utilized cell line and drug-paired data pre-processed by DeepCDR [39], including 223 drugs and 561 cell line bulk gene expression profiles for 697 genes from 31

Table 21: The number of cell samples (#Cells) for the marker gene prediction datasets GSE96583 ( $D_1^{mk}$ ) and GSE130148 ( $D_2^{mk}$ ).

Dataset	GSE96583_1	GSE96583_2	GSE96583_3	GSE96583_4	GSE96583_5	GSE130148
#Cells	4,246	3,639	14,619	14,446	6,145	10,360

Table 22: The correlation of the ontology structure and the pairwise similarity of known cell type representations

Method	Spearman R $\uparrow$
<b>Non-TFM Methods</b>	
Raw Data	0.212
Seurat	<u>0.316</u>
Harmony	0.262
<b>Ontology-Agnostic TFMs</b>	
Geneformer	0.284
scGPT	0.037
scTab	0.209
UCE	0.285
MGP	0.275
Sup	0.229
MGP+Sup	0.238
<b>Ontology-Enhanced TFMs</b>	
<b>scCello</b>	<b>0.506</b>

different cancer types. Among the dataset, 89,585 cell line-drug samples were used for training and 4,729 for testing [25].

**Hyper-parameters.** We following scFoundation’s implementation to set the parameters in the DeepCDR framework, like “-use\_gexp” as True, and both “-use\_mut” and “-use\_methy” as False.

**Performance.** Results are already reported in Tab. 4 in Sec. 4.5.

## D.6 Batch Integration

**Method.** This batch integration task aims to seamlessly integrate scRNA-seq data from different batches, which can be conducted using the same protocol as cell type clustering. After clustering, model performance is evaluated. Besides using cell type labels and clustering indices from the optimized Louvain algorithm to calculate the preservation of biological signals (NMI, ARI, ASW and AvgBio), this task also use batch labels to measure the removal of batch effects (ASW<sub>b</sub> and AvgBatch). See App. D.1 for metric calculation details.

**Datasets.** As introduced in Sec. 4.6, all datasets used in the cell type clustering task (Sec. 4.2.1) are evaluated, including one ID dataset  $D^{id}$  and six OOD datasets  $D_i^{cond}$  ( $cond \in \{ct, ts, dn\}$ ,  $i \in \{1, 2\}$ ).

**Hyper-parameters.** We use the same hyper-parameters as that in cell type clustering.

**Performance.** In Sec. 4.6, the Overall score, a weighted average of AvgBio and AvgBatch, is already reported in Fig. 3. Complete results for all metrics are included in Tab. 23 for the ID dataset  $D^{id}$ , Tab. 24 for the OOD cell type datasets  $D_1^{ct}$  and  $D_2^{ct}$ , Tab. 25 for the OOD tissue datasets  $D_1^{ts}$  and  $D_2^{ts}$ , and Tab. 26 for the OOD donor datasets  $D_1^{dn}$  and  $D_2^{dn}$ .



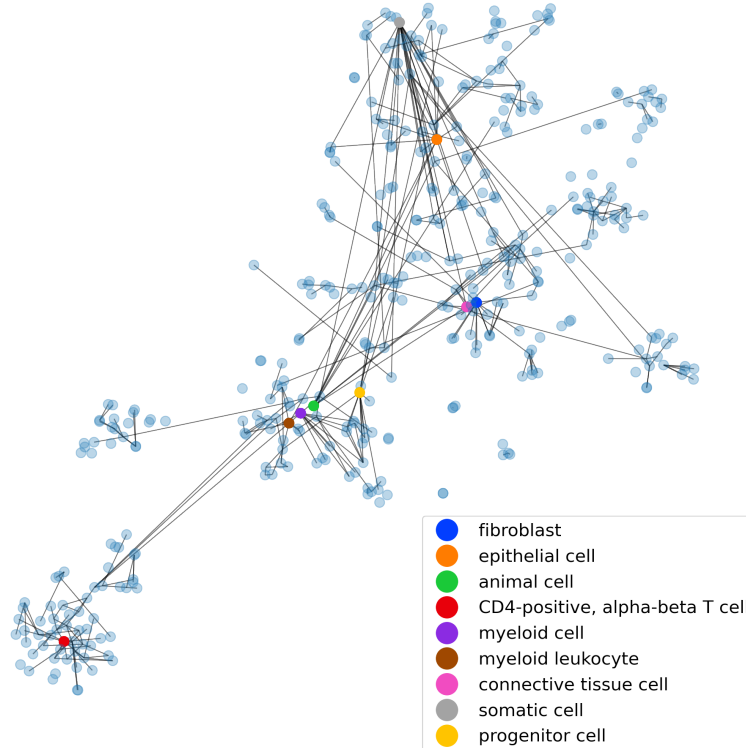


Figure 11: Visualization for learned cell representations of scCello (introduced in App. D.7). The nodes are different cell types in the pre-training dataset and the edges denote "is a subtype of" relationships in cell ontology  $\mathcal{G}$ . The coordinates of nodes are calculated using tSNE dimensional reduction for cell type representations derived from scCello. As expected, highly ontology-correlated cell type pairs are very close in the latent space, such as myeloid leukocyte and myeloid cell, as well as fibroblast and connective tissue cell. Meanwhile, dissimilar cell type pairs remain distant, such as CD4-positive, alpha-beta T cell and epithelial cell. The highly biologically informative representation space implies scCello’s potential generalization ability to other cell-type-related downstream tasks.

## D.7 Visualization for Learned Cell Representations

We calculate known cell type representation as introduced in Sec. D.3, by averaging cell representations for each type on 10% of the pre-training data. Then we apply tSNE to project the known cell type representations to 2D space and visualize in Fig. 11. Highly correlated cell types are clustered together as expected, and dissimilar cell types are distant.

We also calculate the Spearman R correlation of the pairwise similarity of known cell type representations and the ontology structure (1 for an edge between two cell types and 0 for no edge between them) in Tab. 22. As expected, scCello learned a biologically informative representation space that is much more correlated to the true ontology structure than other methods. This implies scCello’s potential generalization ability to other cell-type-related downstream tasks.

Table 23: Batch integration on ID dataset  $D^{id}$ .

Method	ID Unseen Data ( $D^{in}$ )				
	ASW <sub>b</sub> ↑	GraphConn↑	AvgBatch↑	AvgBio↑	Overall↑
<b>Non-TFM Methods</b>					
Raw Data	<b>0.951</b>	0.806	<u>0.878</u>	0.419	0.603
Seurat	0.829	0.686	<u>0.757</u>	0.442	0.568
Harmony	0.824	0.688	0.756	0.421	0.555
scVI	0.880	0.738	0.809	0.474	0.608
<b>Ontology-Agnostic TFMs</b>					
Geneformer	0.875	0.676	0.775	0.432	0.569
scGPT	0.887	0.691	0.789	0.438	0.578
scTab	<u>0.917</u>	<b>0.925</b>	<b>0.921</b>	<u>0.577</u>	<b>0.715</b>
UCE	0.906	0.788	0.847	0.489	0.632
MGP	0.870	0.728	0.799	0.473	0.603
Sup	0.885	0.809	0.847	0.555	0.672
MGP+Sup	0.892	<u>0.829</u>	0.860	0.516	0.654
<b>Ontology-Enhanced TFMs</b>					
<b>scCello</b>	0.834	0.697	0.766	<b>0.670</b>	<u>0.708</u>

Table 24: Batch integration on OOD cell type datasets  $D_1^{ct}$  and  $D_2^{ct}$ .

Method	OOD CellType Data ( $D_1^{ct}$ )					OOD CellType Data ( $D_2^{ct}$ )				
	ASW <sub>b</sub> ↑	GraphConn↑	AvgBatch↑	AvgBio↑	Overall↑	ASW <sub>b</sub> ↑	GraphConn↑	AvgBatch↑	AvgBio↑	Overall↑
<b>Non-TFM Methods</b>										
Raw Data	<b>0.934</b>	0.940	<b>0.937</b>	0.703	0.797	<b>0.939</b>	0.895	<b>0.917</b>	0.629	0.744
Seurat	0.831	0.928	0.880	0.752	0.803	0.844	0.932	0.888	0.737	0.797
Harmony	0.909	0.800	0.855	0.432	0.601	0.898	0.817	0.858	0.417	0.593
scVI	0.875	<b>0.959</b>	<u>0.917</u>	<u>0.760</u>	<b>0.823</b>	0.880	<b>0.952</b>	<b>0.916</b>	0.725	0.801
<b>Ontology-Agnostic TFMs</b>										
Geneformer	<u>0.915</u>	0.907	0.911	0.689	0.778	0.915	0.917	<b>0.916</b>	0.668	0.767
scGPT	<u>0.903</u>	0.913	0.908	0.707	0.787	0.896	0.927	<b>0.912</b>	0.720	0.797
scTab	0.908	0.904	0.906	0.759	0.818	0.910	0.905	0.908	0.726	0.799
UCE	0.867	0.947	0.907	<b>0.772</b>	<b>0.826</b>	0.854	<u>0.946</u>	0.900	0.741	<u>0.805</u>
MGP	0.894	0.903	0.899	0.714	0.788	<u>0.925</u>	0.580	0.753	0.740	0.745
Sup	0.879	0.944	0.912	<b>0.767</b>	<b>0.825</b>	0.879	0.914	0.897	<u>0.775</u>	<b>0.824</b>
MGP+Sup	0.885	<u>0.946</u>	0.916	0.758	<b>0.821</b>	0.885	0.925	0.905	0.764	<b>0.820</b>
<b>Ontology-Enhanced TFMs</b>										
<b>scCello</b>	0.877	0.911	0.894	<b>0.769</b>	<u>0.819</u>	0.858	0.884	0.871	<b>0.786</b>	<b>0.820</b>

Table 25: Batch integration on OOD tissue datasets  $D_1^{ts}$  and  $D_2^{ts}$ .

Method	OOD Tissue Data ( $D_1^{ts}$ )					OOD Tissue Data ( $D_2^{ts}$ )				
	ASW <sub>b</sub> ↑	GraphConn↑	AvgBatch↑	AvgBio↑	Overall↑	ASW <sub>b</sub> ↑	GraphConn↑	AvgBatch↑	AvgBio↑	Overall↑
<b>Non-TFM Methods</b>										
Raw Data	<b>0.941</b>	0.792	0.867	0.540	0.671	<b>0.946</b>	0.862	0.904	0.631	0.740
Seurat	0.865	0.830	0.847	0.587	0.691	0.867	0.841	0.854	0.636	0.723
Harmony	0.905	0.755	0.830	0.462	0.609	0.908	0.744	0.826	0.515	0.639
scVI	0.901	0.861	0.881	0.577	0.699	0.910	0.881	0.896	0.634	0.739
<b>Ontology-Agnostic TFMs</b>										
Geneformer	<u>0.925</u>	0.804	0.865	0.539	0.669	<u>0.924</u>	0.835	0.880	0.597	0.710
scGPT	0.916	0.776	0.846	0.544	0.665	0.920	0.826	0.873	0.627	0.725
scTab	0.916	0.872	<u>0.894</u>	0.515	0.667	0.917	0.874	0.896	0.657	0.753
UCE	0.905	0.864	0.885	0.598	<u>0.713</u>	0.911	0.879	0.895	0.670	0.760
MGP	0.887	0.887	0.887	0.576	0.700	0.901	0.815	0.858	0.628	0.720
Sup	0.903	<u>0.932</u>	<b>0.918</b>	<u>0.605</u>	<b>0.730</b>	0.899	<u>0.911</u>	<b>0.905</b>	<u>0.680</u>	<b>0.770</b>
MGP+Sup	0.900	<b>0.941</b>	<b>0.921</b>	<b>0.610</b>	<b>0.734</b>	0.898	<b>0.922</b>	<b>0.910</b>	0.672	<b>0.767</b>
<b>Ontology-Enhanced TFMs</b>										
<b>scCello</b>	0.868	0.841	0.855	<b>0.612</b>	0.709	0.884	0.819	0.852	<b>0.705</b>	<u>0.764</u>

Table 26: Batch integration on OOD donor datasets  $D_1^{dn}$  and  $D_2^{dn}$ .

Method	OOD Donor Data ( $D_1^{dn}$ )					OOD Donor Data ( $D_2^{dn}$ )				
	ASW $_b$ ↑	GraphConn↑	AvgBatch↑	AvgBio↑	Overall↑	ASW $_b$ ↑	GraphConn↑	AvgBatch↑	AvgBio↑	Overall↑
<b>Non-TFM Methods</b>										
Raw Data	<b>0.945</b>	0.785	0.865	0.458	0.621	<b>0.946</b>	0.787	0.867	0.460	0.623
Seurat	0.875	0.759	0.817	0.466	0.606	0.876	0.771	0.824	0.489	0.623
Harmony	0.893	0.618	0.756	0.456	0.576	0.891	0.655	0.773	0.474	0.594
scVI	0.914	0.831	0.872	0.478	0.636	0.909	0.837	0.873	0.502	0.650
<b>Ontology-Agnostic TFMs</b>										
Geneformer	0.921	0.763	0.842	0.468	0.618	0.919	0.768	0.844	0.482	0.627
scGPT	0.920	0.757	0.839	0.456	0.609	0.920	0.763	0.842	0.477	0.623
scTab	/	/	/	OOM	OOM	/	/	/	OOM	OOM
UCE	0.904	0.665	0.784	0.485	0.605	0.907	0.558	0.733	0.506	0.597
MGP	0.910	0.824	0.867	0.488	0.640	0.906	0.814	0.860	0.518	0.655
Sup	0.909	0.877	0.893	0.552	0.688	0.902	0.857	0.880	0.573	0.696
MGP+Sup	0.910	<b>0.888</b>	<b>0.899</b>	0.553	<b>0.691</b>	0.903	<b>0.869</b>	<b>0.886</b>	0.570	0.696
<b>Ontology-Enhanced TFMs</b>										
scCello	0.845	0.805	0.825	<b>0.608</b>	<b>0.695</b>	0.849	0.802	0.826	<b>0.643</b>	<b>0.716</b>